VACCINES

Polymer nanoparticles deliver mRNA to the lung for mucosal vaccination

Alexandra Suberi[1], Molly K. Grun[2], Tianyang Mao[3], Benjamin Israelow[3,4], Melanie Reschke[5]†, Julian Grundler[6], Laiba Akhtar[2], Teresa Lee[1], Kwangsoo Shin[1]‡, Alexandra S. Piotrowski-Daspit[1]§, Robert J. Homer[7], Akiko Iwasaki[3,8], Hee-Won Suh[1]*, W. Mark Saltzman[1,2,9,10]*

An inhalable platform for messenger RNA (mRNA) therapeutics would enable minimally invasive and lung-targeted delivery for a host of pulmonary diseases. Development of lung-targeted mRNA therapeutics has been limited by poor transfection efficiency and risk of vehicle-induced pathology. Here, we report an inhalable polymer-based vehicle for delivery of therapeutic mRNAs to the lung. We optimized biodegradable poly(-amine-*co*-ester) (PACE) polyplexes for mRNA delivery using end-group modifications and polyethylene glycol. These polyplexes achieved high transfection of mRNA throughout the lung, particularly in epithelial and antigen-presenting cells. We applied this technology to develop a mucosal vaccine for severe acute respiratory syndrome coronavirus 2 and found that intranasal vaccination with spike protein–encoding mRNA polyplexes induced potent cellular and humoral adaptive immunity and protected susceptible mice from lethal viral challenge. Together, these results demonstrate the translational potential of PACE polyplexes for therapeutic delivery of mRNA to the lungs.

INTRODUCTION

mRNA-based vaccines for severe acute respiratory syndrome coronavirus 2 (SARS-CoV-2) have demonstrated the potential of mRNA therapeutics for safe and effective use in the general population (*1*, *2*). The long-anticipated development of mRNA vaccines was enabled by critical advancements in mRNA technology that improved stability and transfection while minimizing innate immune activation (*3*). To capitalize on these advancements and expand the application of mRNA therapeutics beyond delivery of systemically administered vaccines, further research and development is required to optimize mRNA delivery vehicles for diverse applications in vivo (*4*, *5*). Delivery vehicles protect highly degradable mRNA cargos and promote cellular uptake and protein expression. An optimized vehicle has the potential to deliver diverse mRNA sequences, or combinations of mRNA sequences, enabling applications for a broad range of prophylactic and therapeutic treatments without extensive reformulation.

[1]Department of Biomedical Engineering, Yale University, New Haven, CT 06511, USA. [2]Department of Chemical and Environmental Engineering, Yale University, New Haven, CT 06511, USA. [3]Department of Immunobiology, Yale University School of Medicine, New Haven, CT 06519, USA. [4]Department of Medicine, Section of Infectious Diseases, Yale University School of Medicine, New Haven, CT 06519, USA. [5]Department of Molecular Biophysics and Biochemistry, Yale University, New Haven, CT 06520, USA. [6]Department of Chemistry, Yale University, New Haven, CT 06511, USA. [7]Department of Pathology, Yale University School of Medicine, CT 06510, USA. [8]Howard Hughes Medical Institute, Chevy Chase, MD 20815, USA. [9]Department of Cellular and Molecular Physiology, Yale School of Medicine, New Haven, CT 06510, USA. [10]Department of Dermatology, Yale School of Medicine, New Haven, CT 06510, USA.
*Corresponding author. Email: heewon.suh@yale.edu (H.W.S.); mark.saltzman@yale.edu (W.M.S.)
†Present address: Emerald Cloud Lab, Astoria, NY 11103, USA.
‡Present address: Department of Polymer Science and Engineering and Program in Environmental and Polymer Engineering, Inha University, Incheon, Republic of Korea.
§Present address: Department of Biomedical Engineering, University of Michigan, Ann Arbor, MI, USA; Department of Internal Medicine, Pulmonary and Critical Care Medicine Division, University of Michigan, Ann Arbor, MI, USA.

An inhalable or topically administered delivery vehicle would facilitate minimally invasive and lung-targeted therapies for pulmonary pathologies. In particular, inhaled delivery would be ideal for creating improved mucosal vaccines for respiratory pathogens, protein supplementation, or gene editing in the lung (*6*–*9*). Several major limitations have hindered the development of inhaled mRNA therapeutics. First, mRNA delivery vehicle efficacy is highly dependent on the route of administration (*10*) and must therefore be optimized for expression in the lung. Physiologic barriers such as the respiratory mucosal layer, mucociliary clearance into the gastrointestinal tract, and phagocytic cells must be overcome for delivery to target cells in the lungs. High transfection efficiency is required to reduce the therapeutic dose and reach the concentration of protein necessary to achieve a therapeutic response. For example, despite initially promising safety and tolerability, RESTORE-CF—an inhaled mRNA clinical trial, delivering cystic fibrosis transmembrane conductance regulator (CFTR)–encoding mRNA in lipid nanoparticles (LNPs) for treatment of cystic fibrosis (CF)—failed to improve pulmonary function in the second interim report, highlighting the need for improvements in the delivery vehicle (*11*). Another key concern for inhaled therapeutic delivery is that the respiratory mucosa is particularly susceptible to immunopathology (*12*). Several components of the LNP delivery vehicles used in both approved mRNA vaccines have been shown to induce inflammation in the respiratory tract after intranasal administration (*13*). A nanoparticle (NP) optimized for inhaled administration that achieves high mRNA transfection efficiency with minimal induction of an inflammatory immune response is needed to enable development of pulmonary mRNA therapeutics.

We sought to overcome the challenges to delivering mRNA to the lung by creating a topically administered, well-tolerated, polymer-based delivery vehicle. Previously, we demonstrated that a family of biodegradable poly(amine-*co*-ester) (PACE) polymers can encapsulate and protect nucleic acid cargos for delivery in vivo (*14*). The chemical composition of PACE polymers is highly

tunable depending on the monomer components added to the polymerization reaction, the ratios of the components, and synthesis conditions (*15*). For certain polymer compositions, PACE polymers form polyplexes with mRNA (PACE-mRNA) through a combination of electrostatic interactions between the mildly cationic polymer and the negatively charged phosphate backbone of nucleic acids as well as hydrophobic interactions between segments of the polymer chain. PACE polymers can also be modified through the addition of end groups. We have demonstrated that amine-containing end groups can improve transfection efficiency by facilitating endosomal escape of mRNA from the endocytosed NP into the cytoplasm (*16*). Stabilization of PACE-mRNA polyplexes with polyethylene glycol (PEG) can further improve mRNA delivery in vivo (*17*). We capitalized on the highly tunable nature of PACE polyplexes by screening a library of delivery vehicles with different chemical end groups and PEG content to optimize for high protein expression after local delivery to the respiratory tract.

In the present work, we created an optimized PACE-mRNA polyplex delivery vehicle that achieves high protein expression in the lung, primarily in epithelial cells and antigen-presenting cells, with tolerability for repeat dosing and minimal inflammatory response. We demonstrate that our formulation can deliver diverse mRNA cargos to mice, ranging from 1000 to 4000 nucleotides (nt) in length. To demonstrate the translational potential of our delivery vehicle, we created an inhalable spike protein–encoding mRNA vaccine for SARS-CoV-2. Our vaccine induced de novo immunity to SARS-CoV-2 through both systemic and local induction of antibodies. We demonstrated effective draining lymph node germinal center activation, resulting in expansion of spike protein–specific memory B cells and antibody-secreting cells (ASCs). Intranasal vaccination induced circulating antigen–specific $CD8^+$ T cells and lung-resident spike protein–specific tissue memory $CD8^+$ T cells. Last, intranasal PACE-mRNA vaccination protected keratin 18 (K18)–human angiotensin-converting enzyme 2 (hACE2) mice from lethal SARS-CoV-2 challenge.

RESULTS

PACE polymers encapsulate and deliver mRNA to cells

We optimized PACE polyplexes for mRNA delivery to the lung by screening blends that combine the benefits of PEG stabilization and end group–mediated enhanced endosomal escape. We identified 10 promising end-group chemistries and synthesized PACE polymers by enzymatic copolymerization of 15-pentadecanolide, *N*-methyl diethanolamine, and sebacic acid followed by carbonyldiimidazole-mediated conjugation of amine-containing end groups, using a modified literature protocol (Fig. 1A) (*16*). Amine conjugation was performed in two steps: first, by reacting the polymer with carbonyldiimidazole, and, second, reacting with various small molecules containing primary amines. Each conjugation step was monitored by nuclear magnetic resonance spectroscopy (figs. S1 to S3) and gel permeation chromatography (GPC) (fig. S4 and table S1). A PACE block copolymer with PEG (PACE-PEG) was synthesized by adding a 5-kDa methoxy-ended PEG during enzymatic copolymerization, following a modified literature protocol (*15*, *18*). This resulted in a PACE-PEG polymer of 12.2 kDa; the PACE and end group–conjugated PACE polymers were about 4 kDa in average molecular weight (M_n), as characterized by GPC (fig. S4 and table S1).

We administered end group–modified PACE-mRNA to human alveolar epithelial cells (A549) and identified PACE with end group 14 (E14) as a promising candidate for delivery (fig. S5). Next, we examined the effect of PACE-PEG content on polyplex characteristics by blending PACE-E14 and PACE-PEG at different ratios (table S2). PACE-PEG reduced the size and surface charge of PACE-mRNA polyplexes (Fig. 1, B and C), which is consistent with previous reports that PEGylation of cationic polymers can neutralize surface potential (*19*–*21*). mRNA loading efficiency was measured using a fluorescent nucleic acid stain (Quant-iT RiboGreen). Although non-PEGylated polyplexes efficiently loaded mRNA (95% loading), the addition of PACE-PEG improved loading efficiency to around 99% (Fig. 1D), suggesting that incorporating PEG can improve the polyplex formulation process.

To provide greater insight into how PEG content affects polyplex structure, we calculated the PEG density and conformation on the surface of PACE-mRNA polyplexes with 1, 10, or 25% PACE-PEG by determining the polyplex molar mass through static light scattering measurements and by calculating the PEG surface density assuming that 100% of PEG chains are located on the polyplex surface (table S3) (*22*). Polyplexes with PACE-PEG content of 1 to 10% had a surface PEG density in which PEG chains are in a mushroom conformation, with the distance between PEG chains (D) greater than twice the Flory radius of PEG (R_F), whereas 25% PACE-PEG content produces a surface PEG density corresponding to a brush conformation (Fig. 1E).

To compare the mRNA uptake and transfection efficiency of PACE-mRNA polyplexes in vitro, we treated A549 cells with polyplexes loaded with cyanine-5 (Cy5)–labeled enhanced green fluorescent protein (EGFP) mRNA or unlabeled EGFP mRNA using a range of PACE-PEG contents, and we measured the fluorescent signal by microscopy and flow cytometry. Fluorescence microscopy demonstrated that PACE-mRNA without PACE-PEG transfected cells at a comparable rate to a commercial transfection reagent, Lipofectamine MessengerMax (LipoMM). However, we observed a noticeable decrease in EGFP expression at 0.1 and 1% PACE-PEG, although the Cy5-labeled mRNA signal remained consistent (Fig. 1F). By flow cytometry, we observed that, although polyplex uptake (measured by Cy5-mRNA signal) decreased with the addition of PACE-PEG, the overall uptake was still high; even at 10% PACE-PEG concentration, 99.7% of cells were positive for Cy5 (Fig. 1G). By contrast, the average transfection efficiency (measured by EGFP signal) decreased from 85 to 15% with increasing amounts of PACE-PEG (Fig. 1H). Overall, the incorporation of PACE-PEG caused a decrease in mRNA transfection efficiency that outpaced the drop in mRNA uptake (fig. S6). These results suggest that, although PEGylation inhibits the uptake of PACE polyplexes to some degree, lower uptake does not fully explain the inhibitory effect of PEG on mRNA transfection in vitro. On the basis of our prior work demonstrating that mRNA transfection efficiency correlates more strongly with endosomal escape than cellular uptake (*16*), we hypothesize that PEGylation influences the extent of endosomal escape. In support of this, we noted a decrease in cytoplasmic Cy5-mRNA signal as the extent of PEGylation was increased (Fig. 1F).

The biocompatibility of PACE-mRNA polyplexes with 0, 10, and 25% PACE-PEG was compared with that of LipoMM using the neutral red viability assay. A549 cells were treated with a range of mRNA concentrations, delivered with a consistent ratio of

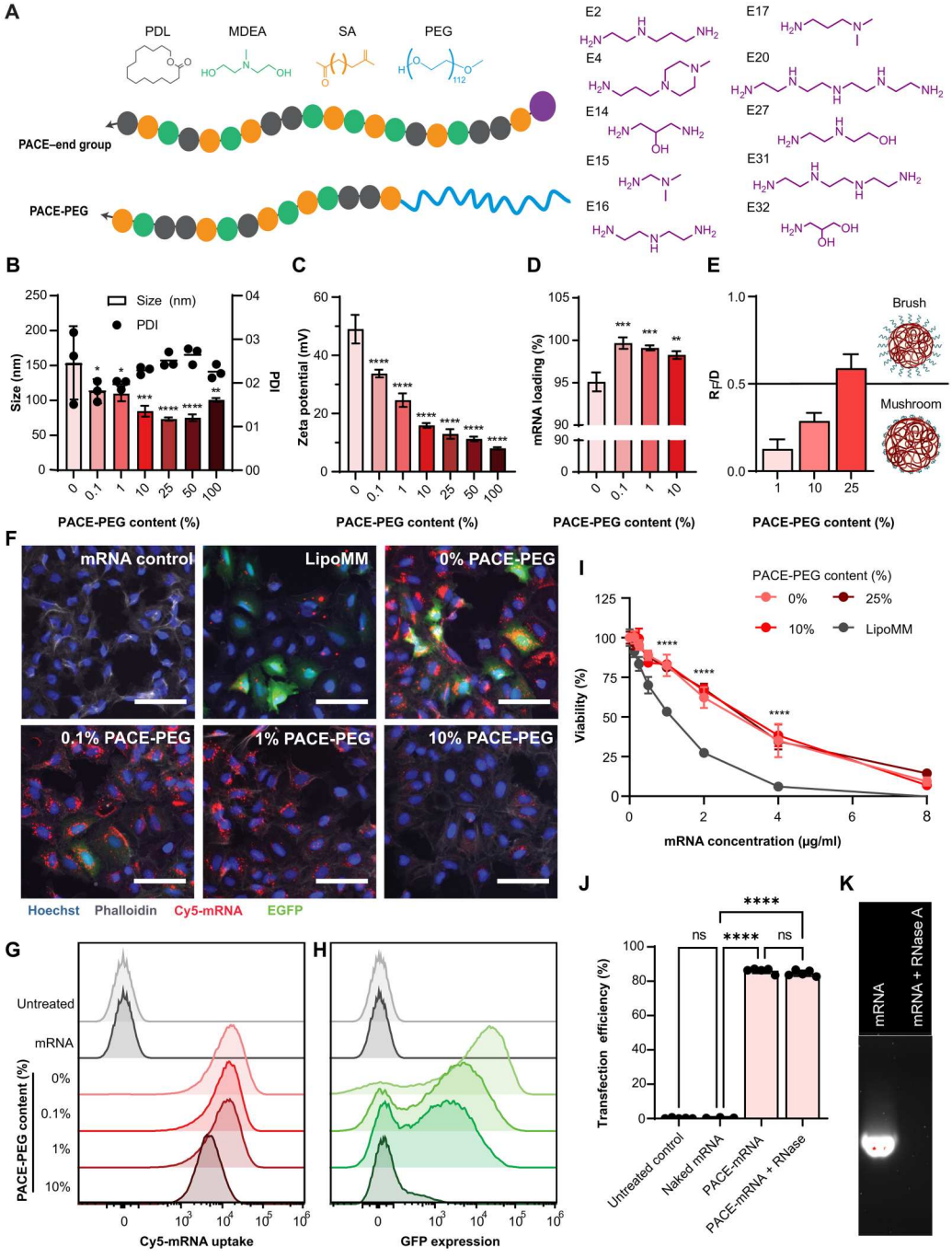

Fig. 1. Characterization of PACE-mRNA polyplexes and in vitro activity. (**A**) Schematic of end group–modified and PEGylated PACE polymer composition with chemical structures of base monomers and end groups. PDL, 15-pentadecanolide; MDEA, *N*-methyl diethanolamine; SA, sebacic acid. (**B** to **E**) Shown are size and polydispersity index (PDI) (B), zeta potential (C), mRNA loading (D), and PEG conformation on the surface of PACE-E14 polyplexes encapsulating EGFP mRNA with varying PACE-PEG content (E). R_F represents PEG Flory radius, and *D* represents the distance between PEG chains. Asterisks indicate statistical difference in size from non-PEGylated polyplexes. Data were analyzed using two-way (A and B) or one-way (C and D) analysis of variance (ANOVA) with Dunnet's multiple comparisons test. (**F**) Representative mRNA uptake and transfection efficiency of cyanine 5 (Cy5)–conjugated EGFP mRNA delivered with PACE-PEG–blended polyplexes or LipoMM (scale bars, 75 μm; Hoechst in blue, phalloidin in gray, Cy5-mRNA in red, and EGFP in green). Naked mRNA delivery to cells is shown as a control. (**G** and **H**) Uptake of Cy5-conjugated mRNA (G) and transfection efficiency of EGFP mRNA (H) are shown for human alveolar epithelial cells (A549) incubated with PEGylated PACE-E14. mRNA indicates cells treated with naked mRNA. (**I**) In vitro cytotoxicity of PEGylated PACE-E14 polyplexes was compared with LipoMM. Asterisks indicate differences between all PACE polyplexes and LipoMM. Data were analyzed using two-way ANOVA with Tukey's multiple comparisons test. (**J** and **K**) Shown are transfection efficiency of EGFP mRNA PACE-E14 polyplexes in human embryonic kidney–293 cells with or without coincubation of RNase (J) and a gel run with either naked mRNA or naked mRNA and RNase showing degradation of mRNA by the enzyme (K). Data were analyzed using one-way ANOVA with Tukey's multiple comparisons test. *$P \leq 0.05$, **$P \leq 0.01$, ***$P \leq 0.001$, and ****$P \leq 0.0001$; ns, not significant. Data are presented as means ± SD. Data are pooled from three independent experiments with one batch of polyplexes per triplicate measurement and $n = 2$ wells per treatment group.

polymer or LipoMM. At higher concentrations, the PACE-mRNA polyplexes were significantly ($P < 0.0001$) less cytotoxic than LipoMM. There was no difference in viability between the polyplexes based on PEG content (Fig. 1I). These results demonstrate the superiority of PACE-mRNA polyplexes compared with LipoMM in achieving comparably high mRNA transfection efficiency with reduced cytotoxicity in vitro.

A primary motivation for encapsulating mRNA into a delivery vehicle is to protect the delicate nucleic acid from abundant degradative enzymes in the lung mucosa. To demonstrate the ability of PACE to protect cargo from ribonuclease (RNase) activity, we coincubated PACE-mRNA polyplexes with RNase before treating human embryonic kidney–293 cells. RNase pretreatment had no effect on transfection efficiency as measured by flow cytometry analysis of the EGFP signal (Fig. 1J). PACE preserved the mRNA

integrity for delivery to cells, whereas naked mRNA was completely degraded after incubation with RNase under identical conditions (Fig. 1K).

Last, the literature suggests that the change in amine to phosphate group ratio per strand on polymer and mRNA, respectively, due to use of differently sized mRNAs can alter the hydrodynamic size and loading capacity (*23*). However, we found that size, zeta potential, and polydispersity index of polyplexes remained consistent when formulated with mRNAs ranging in length from about 1000 to 4000 nt (fig. S7).

Optimization of end-group chemistry and PEG content enhances protein expression in vivo after PACE-mRNA delivery to the lungs

Prior research has established that traditional cell culture methods are not predictive of transfection in vivo for both viral and nonviral delivery systems (*5*, *17*, *24*–*26*). PEGylation of NPs presents additional advantages with administration to mucosal surfaces, because PEGylation is well known to facilitate transport through mucus (*27*), which is not present in most cell cultures. Therefore, despite the reduced transfection efficiency of PEGylated polyplexes observed in vitro, we performed an in vivo screen with PACE-PEG content ranging from 0% (no PACE-PEG) to 100% (no PACE-E14) (table S2). To begin optimizing PACE polyplexes for in vivo lung protein expression, we used intratracheal instillation (IT), an administration method that allows for consistent, rapid, and dose-controlled delivery throughout mouse lungs (*28*–*30*).

We administered 5 μg of firefly luciferase (FLuc) mRNA to mice encapsulated in either PACE polyplexes with varying PEG content or commercially available in vivo transfection agents, JetPEI and GenVoy-ILM (ionizable lipid mix), to assess pulmonary transfection efficiency using a readout of luminescence. At 24 hours, polyplexes formulated with PACE-E14 and 10% PACE-PEG significantly ($P < 0.0001$) outperformed jetPEI and GenVoy-ILM formulations (Fig. 2A and fig. S8A). For PACE-E14 polyplexes, luminescent signal was observed to increase with increasing PACE-PEG content up to 10% PACE-PEG by weight. PACE-PEG content higher than 10% had a progressively inhibitory effect on protein expression, with no luminescent signal observed after delivery of polyplexes made entirely from PACE-PEG (100%) (Fig. 2A). Both PACE-E14 polyplexes (10% PACE-PEG) and GenVoy-ILM particles encapsulating 5 μg of FLuc mRNA were further evaluated for basic biocompatibility by monitoring animal weight for evidence of weight loss and harvesting bronchoalveolar lavage fluid (BALF) at day 14 after delivery. No significant ($P = 0.6664$) differences in animal weights were observed at any time after delivery compared to control sodium acetate (NaAc) buffer–treated animals (fig. S8B), nor was there evidence of sustained recruitment of immune cells to the lung as measured by the white blood cell (WBC) count in the BALF at day 14 for either treatment group (fig. S8C).

We confirmed these results by In Vivo Imaging System (IVIS) imaging, where we observed the highest luminescent signal using 10% PACE-PEG polyplexes (Fig. 2B). We also tracked the luminescent signal after a single delivery over time to see whether PEGylation altered the kinetics of mRNA delivery (fig. S9). Luciferase expression was highest at 6 and 24 hours, which is consistent with previous reports of mRNA expression in the lung (*10*, *31*). These results demonstrate that low amounts of vehicle PEGylation can improve delivery and translation of mRNA, which is consistent with our previous report of mRNA delivery with PACE polyplexes that were not end group–modified (*17*); however, here, we report higher transfection rates, more than 100-fold higher by luminescence, demonstrating the benefit of using end group–modified (E14) PACE.

Next, we performed IVIS imaging of explanted organs (lungs, spleen, liver, kidneys, and heart), which confirmed that IT delivery results in luciferase expression entirely localized in the lungs, with no observable luminescence coming from other organs (Fig. 2C). High luminescent signal was achieved in both left and right lobes of the lung. Using Cy5-labeled mRNA to assess the distribution of IT-delivered PACE-mRNA polyplexes (E14 with 10% PACE-PEG) within the pulmonary architecture, we found PACE-mRNA throughout the large airways and into the alveolar regions of the lung parenchyma (Fig. 2D). We confirmed that our polyplexes could also be delivered by intranasal instillation to achieve high protein expression throughout the lung. We found that both IT and intranasal administration achieve substantial protein expression in all five lung lobes. Whole-mouse imaging demonstrated that intranasal administration resulted in modest luminescent signal in the nasopharynx compared with IT delivery (fig. S10).

Although we had found that E14-modified PACE led to optimal in vitro epithelial cell transfection efficiency, we wondered whether this would hold in vivo. To test the in vivo efficacy of NPs formed from different end group–modified versions of PACE, we performed an additional screen with all 10 end group–modified PACE polymers (Fig. 1A) and a fixed PACE-PEG content of 10% by weight (Fig. 2E). No measurable luminescent signal was observed after administration of 5 μg of naked mRNA in buffer or with polyplexes produced using the base polymer that did not have a conjugated end group. All end group–modified PACE-mRNA polyplexes achieved mRNA expression above control except for E32. We found that E14 remained the top-performing end group for transfection in the lung, consistent with our preliminary cell culture–based screen. However, several other end groups also achieved high protein expression. E27 was identified as a second promising end group for PACE-mRNA polyplexes. We further quantified the amount of luciferase protein per gram of total protein in samples extracted from homogenized lungs by comparing with a standard curve of luminescence with recombinant FLuc protein. Quantification of the two formulations with highest mRNA transfection (E14 and E27 with 10% PACE-PEG) each contained more than 1000 ng of FLuc per gram of protein in the lung (Fig. 2F).

PACE-mRNA polyplexes transfect epithelial cells and antigen-presenting cells in the lung

Having identified two end group–modified PACE polymers (E14 and E27) and the optimal PACE-PEG concentration (10%) for achieving high transfection targeted to the lung, we next characterized cell-type–specific mRNA expression in the lung using Ai14 tdTomato reporter mice. Ai14 mice have a loxP-flanked STOP cassette upstream of a tdTomato gene, which can be excised by Cre-mediated recombination, enabling tdTomato expression in the cell (Fig. 3A). After IT instillation of 10 μg of Cre mRNA in PACE-mRNA polyplexes (E14 with 10% PACE-PEG), 9.97% (SD of 2.32) of all cells in the lung and 28.8% (SD of 12.8) of cells in the BALF expressed tdTomato (Fig. 3B). We further evaluated the lungs to identify endothelial ($CD31^+$), epithelial ($EpCAM^+$), and

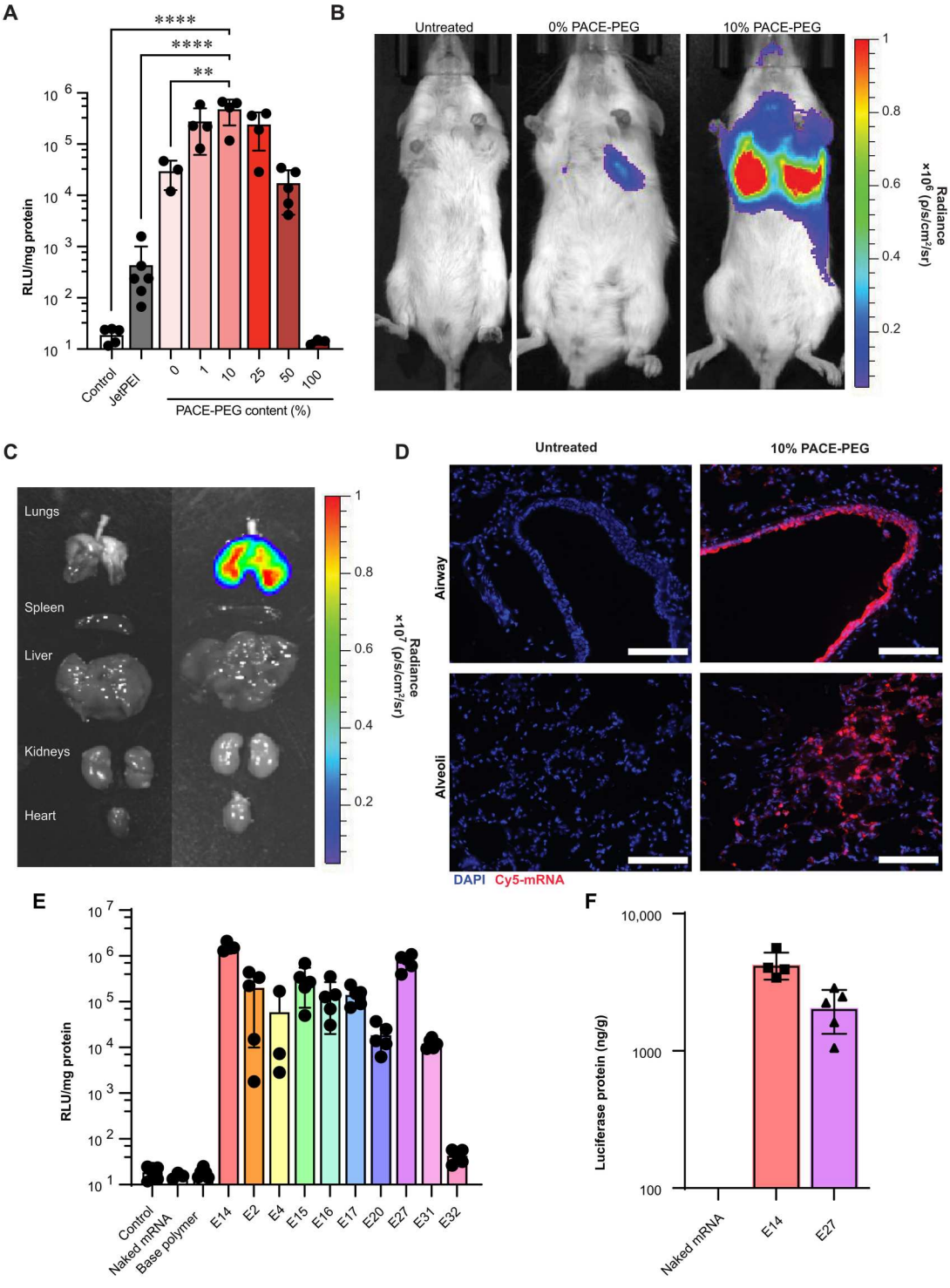

Fig. 2. IT mRNA delivery with PACE-mRNA polyplexes drives protein expression and mRNA distribution throughout the airways and parenchyma. (**A**) Luciferase protein expression was measured in lung tissue after delivery of 5 μg of FLuc mRNA with PEGylated PACE-E14 and in vivo-jetPEI. RLU, relative light units. (**B** and **C**) Representative luciferase expression by IVIS 24 hours after IT delivery of PACE-E14 10% PACE-PEG FLuc mRNA polyplexes in animals (B) and in explanted organs (C). Average radiance units of photons per second per square centimeter per steradian (p/s/cm^2/sr). (**D**) Distribution of Cy5-conjugated mRNA in the lung 30 min after delivery with PACE-E14 polyplexes (scale bars, 150 μm). (**E**) Luciferase protein expression was measured in lung tissue after delivery of FLuc mRNA with polyplexes of various end group–modified PACE and 10% PACE-PEG content, untreated controls, naked mRNA controls, and base polymer with no end-group controls (n = 3 to 5 per group). (**F**) Quantification of luciferase protein extracted from lungs 24 hours after treatment with either E14 or E27 polyplexes with 10% PACE-PEG. Data were analyzed by one-way ANOVA with Tukey's multiple comparisons test of log-transformed sample mean values. Data are presented as means ± SD. Data are pooled from two independent experiments (n = 3 to 6 mice per group). $^{**}P \leq 0.01$ and $^{****}P \leq 0.0001$.

leukocyte (CD45$^+$) subpopulations (fig. S11). Transfection was predominantly achieved in epithelial cells and leukocytes, with 21.5% (SD of 7.32) of lung epithelial cells and 19.6% (SD of 3.47) of lung leukocytes expressing tdTomato. Endothelial cells were not substantially transfected (Fig. 3C). Of the leukocyte cells, we further evaluated markers for antigen-presenting cells in lung tissue. We found that 59.6% (SD of 9.43) of CD11c$^+$CD11b$^+$ cells and 1.04% (SD of 0.28) of CD11c$^+$CD11b$^-$ cells expressed tdTomato. Fluorescence microscopy of lung sections demonstrated that expression of tdTomato could be found primarily in cells lining the conducting airway and throughout the alveolar regions (Fig. 3E). The localization of fluorescence within the lung architecture is consistent with our flow cytometry data showing that transfection occurs primarily in epithelial cells and antigen-presenting cells. We found a similar

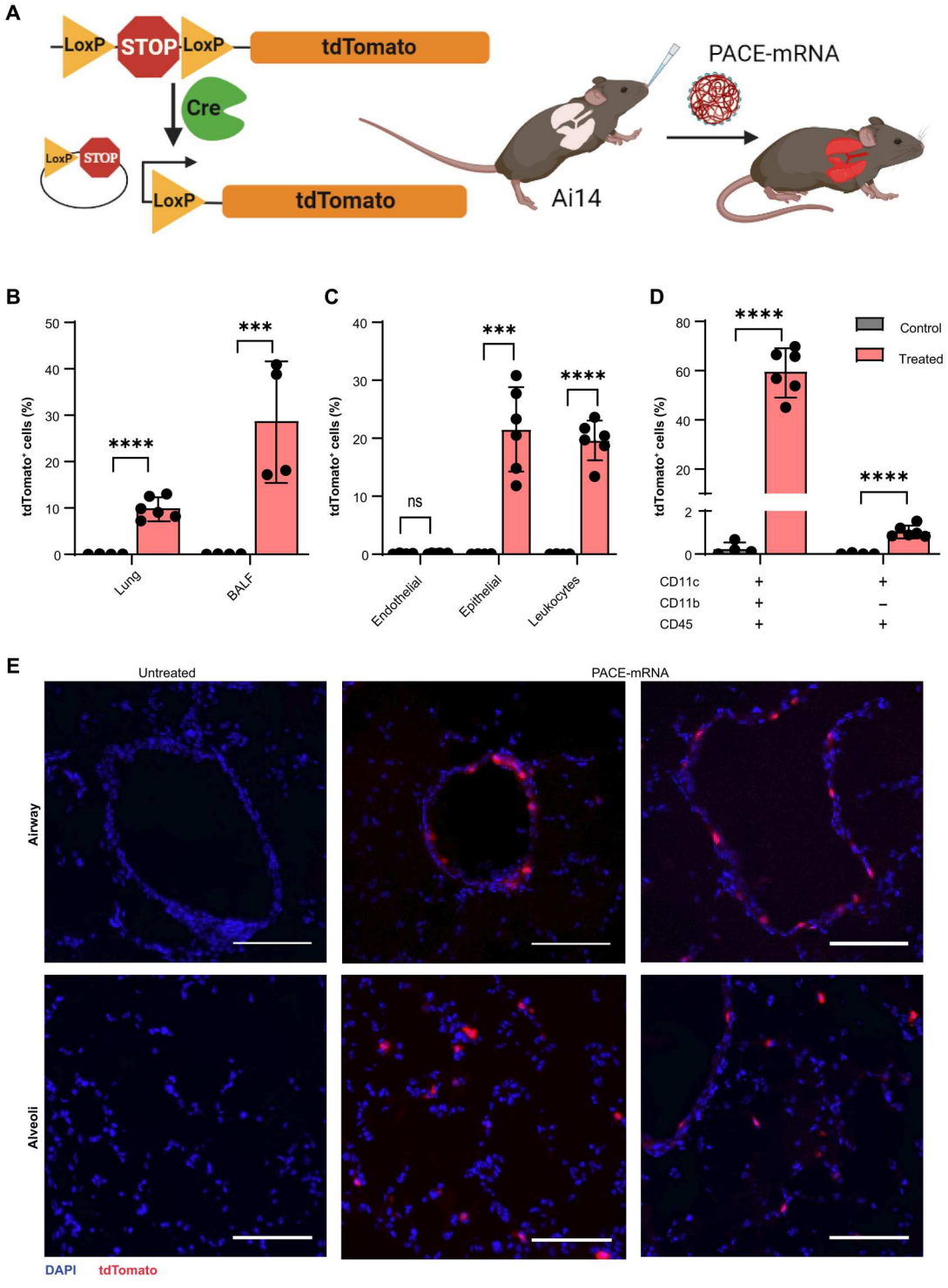

Fig. 3. mRNA expression after IT PACE-mRNA delivery occurs in epithelial cells and antigen-presenting cells. (**A**) Schematic of Cre-mediated recombination in Ai14 mice, resulting in expression of tdTomato protein in transfected cells. (**B** to **D**) Shown are the percent of all live cells in the lung and BALF (B); endothelial, epithelial, or leukocyte cells in the lung (C); and antigen-presenting cells (D) in the lung that expressed tdTomato 24 hours after administration of PACE-E14 polyplexes (10% PACE-PEG) loaded with 10 μg of Cre mRNA. Data are presented as means ± SD. Statistical significance was calculated by multiple unpaired *t* test with Holm-Sidak method. ***$P \leq 0.001$ and ****$P \leq 0.0001$. Data are pooled from two independent experiments ($n = 4$ to 6 per group). (**E**) Shown are representative images of control (untreated) and PACE-E14 polyplex (10% PACE-PEG)–treated lungs from Ai14 mice by fluorescence microscopy [scale bars, 100 μm; 4′,6-diamidino-2-phenylindole (DAPI) in blue; tdTomato in red].

pattern of expression after delivery of E27 polyplexes. Epithelial cells (16.6%, SD of 3.83) and antigen-presenting $CD11c^+CD11b^+$ cells (58.2%, SD of 7.34) were most highly transfected. However, total lung cell transfection was slightly reduced (7.37%, SD of 2.69) (fig. S12).

Many therapeutic applications can be envisioned for targeted mRNA delivery to epithelial cells or antigen-presenting cells. To validate the translational potential of our formulation, we needed to assess the in vivo biocompatibility of polyplexes in the lung. We compared a PACE-mRNA formulation (E14 with 10% PACE-PEG) with buffer-only–treated animals over 14 days. There was no significant ($P = 0.8637$) increase in the leukocyte count in BALF at 14 days after treatment, demonstrating that there is no sustained recruitment of immune cells to the lung (fig. S13A). Mice that received PACE polyplex treatment appeared to exhibit transient weight loss in the first 2 days after treatment but regained that loss within 7 days and then continued to gain weight at a rate comparable to the control group (fig. S13B); however, in a repeat experiment with the same vehicle concentration, PACE polyplex–treated animals did not lose weight (fig. S8B). Serum chemistry measurements demonstrated that there was no elevation in liver enzymes or changes in kidney function at 14 days after treatment (fig. S13, C and D). To further evaluate the acute reaction to PACE polyplex delivery in the lungs, we harvested lungs at 48 hours after treatment. Analysis was performed by a pathologist blinded to the treatment group. Histology of treated lungs showed no evidence of necrosis or other acute airway epithelial change. Some focal areas with mild neutrophilic infiltrate were observed only in the terminal airways in the treatment group (fig. S14). Although this mild focal recruitment of leukocytes observed at 48 hours may be correlated with the initial weight loss, the combination of results including the BALF cell count, normalization of weight gain, and serum chemistries at 14 days supports the overall tolerability of polyplexes for further evaluation with therapeutic mRNAs.

Intranasal PACE-mRNA vaccination induces antigen-specific B and T cell immune responses in the MLN

Next, we sought to assess whether our top-performing PACE-mRNA polyplex (E14 with 10% PACE-PEG) could be applied therapeutically as a mucosal vaccine. We encapsulated mRNA encoding the spike protein from SARS-CoV-2 into PACE-mRNA polyplexes. We chose a mouse model, K18-hACE2 mice, which express hACE2 (the entry receptor for SARS-CoV-2) from the mouse cytokeratin 18 promoter. K18-hACE2 mice are commonly used in preclinical studies because of their susceptibility to infection and severe pulmonary disease after SARS-CoV-2 viral challenge (*32*). For initial vaccine testing, we used a prime and boost vaccination strategy, in which mice received a 10-μg dose of PACE-mRNA delivered intranasally on days 0 and 28. This administration technique (*33*, *34*) and prime-boost dosing strategy are the most commonly used for preclinical mucosal vaccination studies.

On day 42 (14 days after boost), we assessed the development of adaptive immunity against the spike protein in the lung-draining lymph node, the mediastinal lymph node (MLN) (Fig. 4A). We assessed the MLN by flow cytometry for the development of germinal center responses with antigen-specific memory and effector B cells and $CD8^+$ T cells, the critical mediators of durable adaptive immunity in the lung (*35*–*37*). We found that PACE-mRNA vaccination increased the size and cellularity of the MLNs (table S4). We stained with a major histocompatibility complex (MHC) class I tetramer to a SARS-CoV-2 spike protein epitope (VNFNFNGL, 539-546) for identification of spike protein–specific T cells and stained B cells with a receptor binding domain (RBD) B cell tetramer. PACE-mRNA vaccination induced an increase in the population of spike protein–specific $CD8^+$ T cells (Fig. 4B) and T follicular helper (T_{FH}) cells in the MLNs (Fig. 4C). T_{FH} cells promote affinity maturation and class switch recombination in B cells and critically orchestrate the development of neutralizing antibody responses (*38*). Parenterally administered mRNA vaccines elicit T_{FH} and germinal center B cells, which strongly correlate with neutralizing antibody production (*39*, *40*). Correspondingly, we observed an expansion of RBD-specific B cells ($CD19^+B220^+Tetramer^+$), class-switched B cells expressing immunoglobulin A (IgA) and IgG ($CD19^+B220^+IgD^-IgM^-$), activated germinal center B cells ($CD19^+B220^+GL7^+$), and ASCs ($CD138^+$) in the MLNs (Fig. 4, D to I). These results demonstrated that PACE-mRNA vaccination induces antigen-specific T and B cell responses in the draining lymph node after mucosal delivery. Furthermore, RBD-specific B cells expressed memory markers, suggesting the potential for the efficacy and durability of the adaptive immune response after PACE-mRNA vaccination.

Intranasal PACE-mRNA vaccination elicits tissue-resident and circulating immunity that protects against SARS-CoV-2 viral challenge

Having demonstrated that PACE-mRNA mucosal vaccination effectively induces an adaptive immune response in the local MLN, we next assessed lung tissues, sera, and BALF for local and systemic antigen-specific T cells and antibodies 14 days after boost (Fig. 5A). We used intravenous (IV) labeling of CD45 to differentiate between circulating and tissue-infiltrating immune cells. Consistent with our findings in the MLNs, we found that vaccination increased the number of spike protein–specific $CD8^+$ T cells in the lung parenchyma (IV^-) (Fig. 5B). Spike protein–specific $CD8^+$ T cells expressed tissue-resident memory (T_{RM}) surface markers, $CD69^+$ and $CD103^+$ (Fig. 5, C and D). We also found significant ($P = 0.0249$) increases in systemic circulating antigen–specific $CD8^+$ T cells harvested from the lungs ($IV^+Tetramer^+CD8^+$) (Fig. 5E). These results demonstrate that vaccination elicited both a lung-resident and a circulating $CD8^+$ T cell response. We assessed sera and BALF for anti-SARS-CoV-2 spike S1 IgG and IgA to determine whether mucosal vaccination induced humoral immunity. We found that both circulating (sera) and mucosal (BALF) IgG antibodies were found at significantly ($P = 0.0286$) higher concentrations (Fig. 5, F and G), but IgA was not (fig. S15).

Last, we assessed whether the cellular and humoral immune response generated by PACE-mRNA vaccination would effectively neutralize SARS-CoV-2 and confer protective immunity to mice. We challenged naïve and PACE-mRNA–vaccinated K18-hACE2 mice with a lethal dose of SARS-CoV-2 isolate hCOV-19/USA-WA1/2020 [6×10^3 plaque-forming units (PFU)] 4 weeks after boost delivery (Fig. 5A). We harvested lungs at 3 days postinfection (DPI) and measured the infectious viral load in the lung tissue by plaque assay to determine whether vaccination successfully reduced the viral burden. We found that PACE-mRNA vaccination significantly ($P = 0.0002$) reduced the viral burden in the lungs of treated animals (Fig. 5H). Likewise, weight loss and survival in vaccinated mice were both improved (Fig. 5, I to K). To further confirm that the protection observed in this vaccination model was due to spike

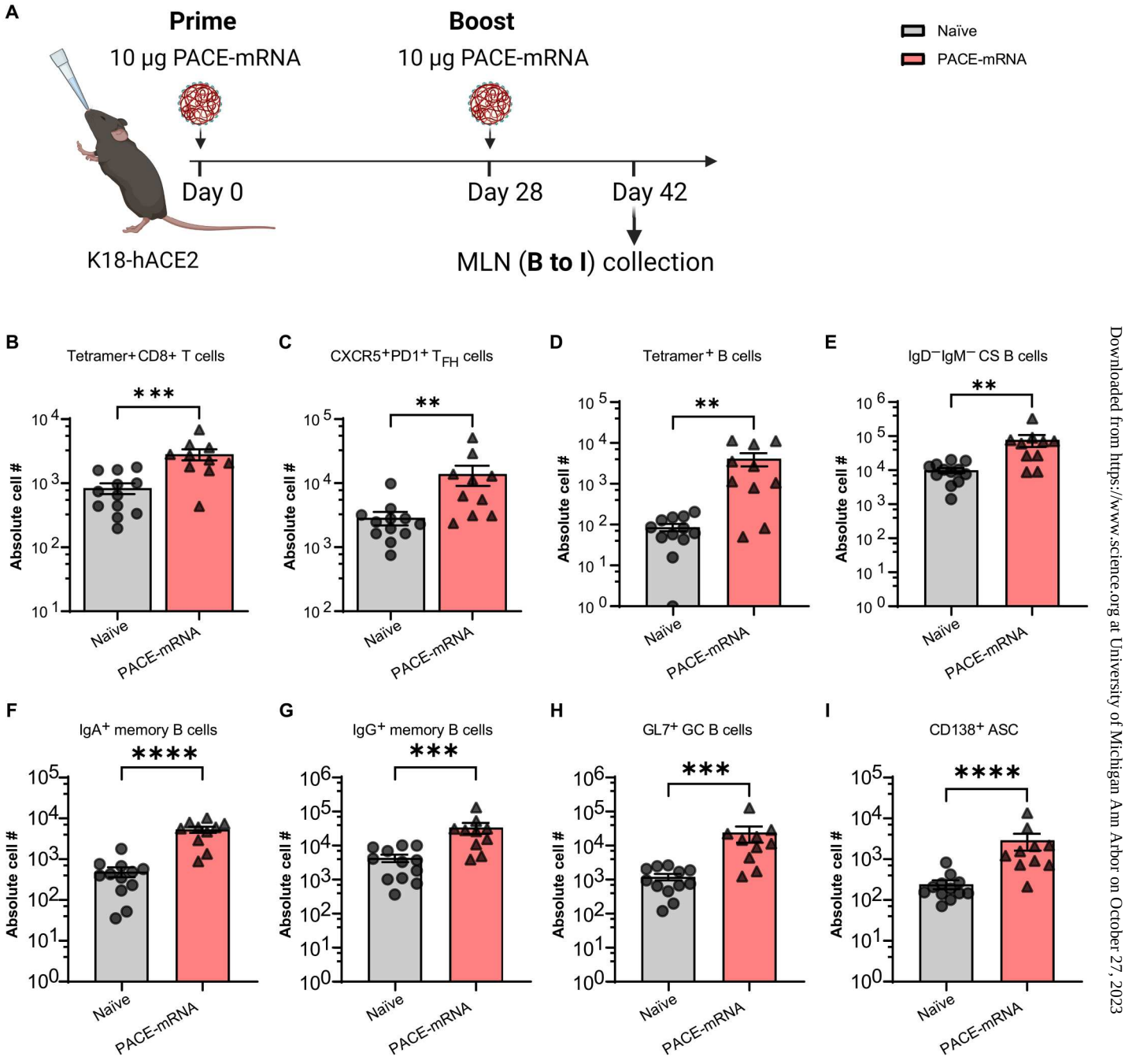

Fig. 4. Intranasal PACE-mRNA vaccination induces antigen-specific T and B cell responses in the draining lymph node. (**A**) Schematic of PACE-mRNA vaccination in K18-hACE2 mice. Mice were primed (day 0) and boosted (day 28) with a 10-µg dose of spike protein–encoding mRNA encapsulated in PACE-E14 polyplexes with 10% PACE-PEG (n = 10 to 12 mice per cohort). MLNs were harvested on day 42 for analysis. (**B**) Quantification of extravascular (IV^-) SARS-CoV-2 spike protein–specific ($Tetramer^+$) $CD8^+$ T cells in MLNs. (**C**) Quantification of extravascular (IV^-) $CXCR5^+PD1^+$ T_{FH} cells in MLNs. (**D** to **I**) Quantification of various extravascular B cell subsets, including RBD tetramer-binding B cells ($Tetramer^+$ B cells) (D), class-switched B cells (IgD^-IgM^- CS B cells) (E), IgA^+ memory B cells (F), IgG^+ memory B cells (G), activated germinal center B cells ($GL7^+$ GC B cells) (H), and antibody-secreting cells in MLNs ($CD138^+$ ASC) (I). Data are presented as means ± SEM. Statistical significance was calculated by Mann-Whitney test. $^{**}P \leq 0.01$, $^{***}P \leq 0.001$, and $^{****}P \leq 0.0001$. Data are pooled from two independent experiments.

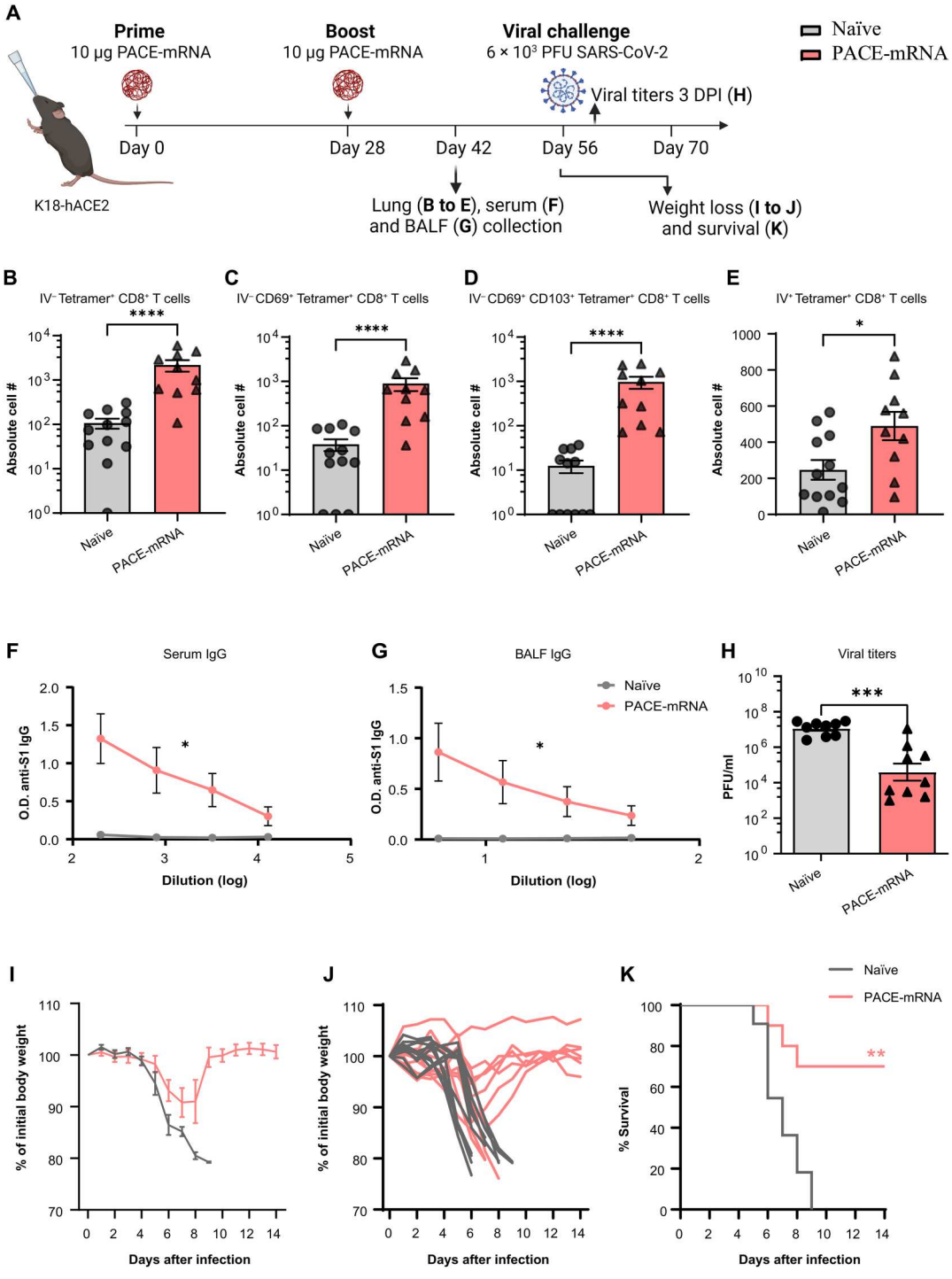

Fig. 5. Intranasal PACE-mRNA vaccination induces protective cellular and humoral immunity. (**A**) Schematic of PACE-mRNA vaccination in K18-hACE2 mice. Mice were primed (day 0) and boosted (day 28) with a 10-µg dose of spike protein–encoding mRNA encapsulated in PACE-E14 polyplexes with 10% PACE-PEG. The lungs, sera, and BALF were harvested on day 42 for analysis (n = 10 to 12 mice per group). Additional groups of vaccinated animals (n = 8 to 10 mice per group) were challenged with 6×10^3 PFU of SARS-CoV-2 on day 56. One group was used for viral titer measurement in lung tissues at 3 DPI. A second group was used to evaluate weight loss and survival over 2 weeks compared with untreated naïve mice. (**B** to **D**) Shown is quantification of extravascular (IV^-) SARS-CoV-2 spike protein–specific ($Tetramer^+$) $CD8^+$ T cells (B), $CD69^+CD103^-Tetramer^+$ $CD8^+$ T cells (C), and $CD69^+CD103^+$ $Tetramer^+$ $CD8^+$ T cells in the lung (D). (**E**) Quantification of circulating (IV^+) SARS-CoV-2 spike protein–specific, $Tetramer^+$ $CD8^+$ T cells from the lung vasculature. (**F** and **G**) Shown is the serum (F) and BALF (G) abundance of SARS-CoV-2 S1 subunit–specific IgG. O.D., optical density. (**H**) Shown are infectious viral titers in lung tissues at 3 DPI as measured by plaque assay. (**I** and **J**) Shown are average (I) and individual (J) weight measurements after viral challenge in naïve and PACE-mRNA–vaccinated mice. (**K**) Shown is survival of naïve and vaccinated mice from 1 to 14 DPI. Data are presented as means ± SEM. Statistical significance was calculated by Mann-Whitney test (B to H) or log-rank Mantel-Cox test (K). *$P \leq 0.05$, **$P \leq 0.01$, ***$P \leq 0.001$, and ****$P \leq 0.0001$. Data are pooled from two independent experiments.

protein–specific immunity rather than a general response to the delivery vehicle, we assessed serum spike protein–specific IgG, viral titers, weight loss, and survival in two additional groups: a vehicle control group that received a prime (day 0) and boost (day 28) with 10 µg of PACE-mRNA (E14 with 10% PACE-PEG) encapsulating FLuc mRNA and a reduced dose vaccination group that received a prime (day 0) and boost (day 28) with 1 µg of PACE-mRNA (E14 with 10% PACE-PEG) encapsulating spike protein–encoding mRNA. We found that the vehicle control group had no evidence of an anti–spike protein immune response demonstrated by the absence of anti-S1 IgG in serum measured by enzyme-linked immunosorbent assay, absence of viral titer reduction in lung tissue harvested 3 DPI, and no improvement in weight loss or survival compared to naïve mice after lethal viral challenge. The 1-µg PACE-mRNA vaccination group demonstrated induction of immunity compared with naïve and vehicle control as demonstrated by

increased serum anti-S1 IgG concentrations and significantly (P = 0.0036) reduced viral load in tissues at 3 DPI (fig. S16).

DISCUSSION

We have demonstrated that PACE polymer formulations can be optimized and applied for local mRNA delivery to the lung. We used a screening method for optimizing polyplexes, a strategy that has previously been used for lipopolyplex (*26*) and LNP (*41*–*44*) optimization. LNP optimization often requires screening varying ratios of four component variables, generating large and unwieldy chemical spaces. Our polyplexes required only two components that facilitated screening efficiency. We showed that a relatively simple polyplex design containing 90% end group–modified PACE (PACE-E14) and 10% PACE-PEG complexed with mRNA to form small and stable polyplexes that protected mRNA from enzymatic degradation and achieved high in vivo transfection efficiency.

By calculating the PEG surface density, we gained insight into how PEG surface density can affect the polyplex structure and mRNA delivery. In general, high PEG density on NPs, achieved by coating the NPs with densely packed linear PEG chains in brush conformation, is desirable to reduce affinity to mucin and enhance mucus-penetrating properties for delivery to the lungs (*45*). We determined that the change in PEG conformation from mushroom to brush conformation occurs around 25% PACE-PEG (or about 10 weight % PEG), which corresponds to an R_F/D value greater than 0.5. At R_F/D greater than 0.5, polyplexes are shielded by a thicker hydrophilic barrier of elongated PEG chains reorganized because of space constraints. Steric repulsion of a PEG shell in the brush conformation decreases the potential for direct interaction between the cell membrane and the cationic core material, such as the amine end groups on PACE-E14. This may explain the inflection in transfection efficiency observed in vivo with increasing PACE-PEG content beyond 10%. Reduction in transfection with increased PEG density is consistent with previous studies demonstrating that increasing PEG surface coverage can interfere with cellular uptake in vivo (*17*, *24*). These results suggest that a degree of PEG coating on a polymeric vehicle can be beneficial for mucosal delivery, but high PEG density results in PEG conformational changes, which can interfere with transfection.

Previous work in both polymer (*46*–*48*) and lipid (*49*, *50*) design has demonstrated that amine-containing end groups can increase mRNA expression or particle targeting to the lung. Our screen identified several amine-containing end groups that increased expression in the lung. The top-performing end groups in our screen (E14 and E27) were not the same end groups that transfected most efficiently after IV administration of unPEGylated PACE-mRNA polyplexes (*16*), supporting the need for compartment-specific optimization of delivery vehicles.

Our optimized PACE polyplexes facilitated mRNA transfection into epithelial cells. Ease of epithelial cell targeting is a primary advantage of inhaled delivery strategies (*31*). Protein replacement therapy by mRNA delivery to epithelial cells is therapeutically relevant for diseases such as CF (*51*, *52*), asthma (*53*), surfactant B protein deficiency (*54*), and alpha-1-antitrypsin deficiency (*55*). Our epithelial transfection rate of greater than 20% after a single dose suggests that protein expression will be therapeutically relevant; prior research has shown that, for disease mitigation, only a fraction of lung cells in CF need to express CFTR. For example, 17 to 28% of cells expressing CFTR in a porcine lung model restored 50% of normal CFTR function, an amount consistent with amelioration of symptoms (*56*). Previous attempts to deliver inhaled mRNA in preclinical models (*57*, *58*) have achieved moderate success in disease treatment, demonstrating both a proof of concept for mRNA as a therapeutic and the need for further innovation. The epithelial protein expression and the tolerability of repeated doses of the PACE vehicles described here support further investigation for protein supplementation applications in the lung.

Vaccination has been a long-standing and heavily researched application for mRNA therapeutics. The unprecedented success of SARS-CoV-2 mRNA vaccines—in terms of efficacy, speed of development, and Food and Drug Administration approval—has established the translational potential of mRNA vaccines. However, new viral variants and waning immunity over time have necessitated the development of vaccine boosters and new treatment modalities (*59*–*64*). Current mRNA vaccination strategies are focused on eliciting systemic immunity, primarily through the induction of IgG antibodies in serum and circulating antigen–specific T cells (*65*, *66*). However, growing evidence supports the potential superior effectiveness of vaccines that are delivered directly to the respiratory tract to combat respiratory viruses (*33*, *67*). The respiratory tract is the site of invasion and the primary site of replication and disease manifestation for SARS-CoV-2 and other respiratory pathogens. By recruiting adaptive immune responses to the respiratory tract, mucosal vaccines could improve protective immunity and reduce viral transmission, potentially stopping infection earlier in its course (*68*, *69*). Several studies investigating viral vector- and protein-based vaccines have demonstrated that superior mucosal immunity can be achieved through direct antigen presentation across the mucosal surface of the lung (*33*, *34*, *70*, *71*). We applied our PACE-mRNA system to create an intranasal vaccine capable of eliciting de novo immunity in mice.

The first steps in developing immunity after mRNA vaccination are antigen protein expression, processing, and presentation by antigen-presenting cells to educate and activate B cells and T cells in the lymph nodes. We showed that a population of lung antigen-presenting cells expressed protein after PACE-mRNA delivery to the lungs in a tdTomato reporter model. Correspondingly, we found that PACE-mRNA vaccination resulted in activation of CD8 T cells, T_{FH} cells, and various B cell subtypes in the MLN, suggesting migration of antigen-presenting cells from the lung to the MLN.

Although class-switched, IgA^+ memory, and IgG^+ memory B cells were both increased in the MLN compared with the naïve group, this did not correspond with IgA secretion in BALF of the vaccinated animals. These results suggest that the PACE-mRNA vaccine formulation or dosing could be further optimized to improve the mucosally secreted antibody response. The presence of populations of IgA^+ memory B cells in the MLN but the absence of IgA secretion in mucus indicates that an additional signal may be required to effectively recruit existing B cells to the lung and stimulate antibody secretion into the respiratory lumen (*72*). Despite the absence of secreted IgA, vaccinated animals did have increased antigen-specific IgG in BALF, demonstrating that this mucosal vaccine leads to the induction of antibodies within the mucosa. Another primary goal of mucosal vaccination is the induction of lung-resident memory $CD8^+$ T cells. These cells occupy the parenchyma of the lung for long periods of time and can

monitor for and quickly respond to viral infection (*73*). PACE-mRNA vaccination resulted in induction of an antigen-specific, lung-localized T_{RM} population. Currently available intramuscularly administered vaccines induce circulating memory T cells, but not lung-resident, spike protein–specific T_{RM} responses (*35*, *74*), highlighting an advantage of our mucosal PACE-mRNA delivery strategy. Although inhaled mRNA has been investigated for prophylactic therapeutics or decoy treatments to fight SARS-CoV-2 (*48*, *75*–*78*), this work is important because it describes de novo induction of protective immunity against SARS-CoV-2 with intranasal delivery of a nonviral vector mRNA vaccine.

Our study has limitations. We used a limited number of animals per group, and differences in some parameters, such as WBC count and related immune responses, will likely be more apparent with inclusion of more animals. Furthermore, we studied responses only in mice, and it will be necessary to repeat this study in larger animal models. We used intranasal and intratracheal delivery, which are well-established methods for administration in mice, but there is a need to explore alternate delivery mechanisms, such as those provided by mucosal atomization or nebulization devices.

In summary, PACE-mRNA polyplexes can be formulated with blends of end group–modified PACE and PACE-PEG to form small, consistent, and stable polyplexes. PACE polyplexes demonstrated favorable tolerability and protected mRNA from degradative enzymes. PEG content can improve polyplex characteristics; however, dense PEG shells can interfere with transfection efficiency. Therefore, PEG content was optimized for lung-specific delivery. Inhaled PACE-mRNA administration achieved high protein expression and effective lung targeting. Transfection occurred primarily in lung epithelial cells and antigen-presenting cells, two cell types that are relevant targets for pulmonary diseases. Last, mucosal vaccination with PACE-mRNA induced systemic and lung-resident adaptive immunity and protected mice from a lethal SARS-CoV-2 challenge. Together, these results highlight the potential of PACE-mRNA polyplexes as a method to deliver mRNAs to the lung.

MATERIALS AND METHODS

Study design

The objective of this study was to optimize a polymer-based mRNA delivery vehicle for delivery to the lungs and to provide a proof of concept for the translational potential of our vehicle as a platform for mucosal vaccination against a respiratory pathogen. We optimized PACE-mRNA by formulating various PACE-mRNA polyplexes with blends of different PACE polymers and screening for luminescent signal in the lungs after intratracheal delivery of PACE-mRNA encoding FLuc. We evaluated the efficacy of our vehicle as a mucosal vaccine by delivering spike protein encoding mRNA and analyzing lung tissues, MLNs, and sera for spike-specific cellular and humoral immunity. We also assessed for functional immunity by challenging mice with SARS-CoV-2 and assessing viral neutralization in the lungs, weight loss, and survival. For controls, in studies evaluating for luminescent signal in the lung, we compared PACE-mRNA treatment with untreated, naked mRNA and two commercially available nonviral mRNA transfection agents, JetPEI and Genvoy-ILM. For vaccination group controls, we compared PACE-mRNA–vaccinated mice with untreated naïve mice and mice treated with a vehicle control that encapsulated a nonantigenic mRNA sequence, FLuc mRNA. All animal experiments were performed in accordance with the protocols approved by the Institutional Animal Care and Use Committees of Yale University. Age- and sex-matched animals were randomly assigned to treatment or control groups for each experiment. No statistical methods were used to predetermine sample sizes. Sample sizes were empirically determined on the basis of previously published work and to ensure sufficient statistical power. Investigators were not blinded to experimental groups because measurements were not subjective except for histologic analysis and viral titer experiments. Data collection was performed with investigators blinded to the experimental group while counting viral plaques. For histology, slides were evaluated by a pathologist blinded to the experimental group. No data were excluded from analysis or corresponding figures. Data including sample sizes, experimental replicates, and statistics are provided in data files S1 and S2 and in the corresponding figures and legends.

Statistical analysis

All raw, individual-level data for experiments where $n < 20$ are presented in data file S1 for Figs. 1 to 5 and data file S2 for the supplementary figures. Results were analyzed using GraphPad Prism (version 9.2.0 for Windows). Data are presented as indicated in the figure legends as either means ± SD or means ± SEM. Figure legends indicate the type of analysis performed for each experiment. Values were considered significantly different at $P < 0.05$.

Supplementary Materials

This PDF file includes:
Materials and Methods
Figs. S1 to S17
Tables S1 to S4
References (*79*–*85*)

Other Supplementary Material for this manuscript includes the following:
Data files S1 and S2
MDAR Reproducibility Checklist

REFERENCES AND NOTES

1. F. P. Polack, S. J. Thomas, N. Kitchin, J. Absalon, A. Gurtman, S. Lockhart, J. L. Perez, G. Pérez Marc, E. D. Moreira, C. Zerbini, R. Bailey, K. A. Swanson, S. Roychoudhury, K. Koury, P. Li, W. V. Kalina, D. Cooper, R. W. Frenck Jr., L. L. Hammitt, Ö. Türeci, H. Nell, A. Schaefer, S. Ünal, D. B. Tresnan, S. Mather, P. R. Dormitzer, U. Şahin, K. U. Jansen, W. C. Gruber, Safety and efficacy of the BNT162b2 mRNA Covid-19 vaccine. *N. Engl. J. Med.* **383**, 2603–2615 (2020).
2. L. R. Baden, H. M. El Sahly, B. Essink, K. Kotloff, S. Frey, R. Novak, D. Diemert, S. A. Spector, N. Rouphael, C. B. Creech, J. McGettigan, S. Khetan, N. Segall, J. Solis, A. Brosz, C. Fierro, H. Schwartz, K. Neuzil, L. Corey, P. Gilbert, H. Janes, D. Follmann, M. Marovich, J. Mascola, L. Polakowski, J. Ledgerwood, B. S. Graham, H. Bennett, R. Pajon, C. Knightly, B. Leav, W. Deng, H. Zhou, S. Han, M. Ivarsson, J. Miller, T. Zaks, Efficacy and safety of the mRNA-1273 SARS-CoV-2 vaccine. *N. Engl. J. Med.* **384**, 403–416 (2021).
3. N. Pardi, M. J. Hogan, F. W. Porter, D. Weissman, mRNA vaccines - a new era in vaccinology. *Nat. Rev. Drug Discov.* **17**, 261–279 (2018).
4. P. S. Kowalski, A. Rudra, L. Miao, D. G. Anderson, Delivering the messenger: Advances in technologies for therapeutic mRNA delivery. *Mol. Ther.* **27**, 710–728 (2019).
5. A. S. Piotrowski-Daspit, A. C. Kauffman, L. G. Bracaglia, W. M. Saltzman, Polymeric vehicles for nucleic acid delivery. *Adv. Drug Deliv. Rev.* **156**, 119–132 (2020).
6. M. Y. T. Chow, R. Y. K. Chang, H. K. Chan, Inhalation delivery technology for genome-editing of respiratory diseases. *Adv. Drug Deliv. Rev.* **168**, 217–228 (2021).
7. M. Y. T. Chow, Y. Qiu, J. K. W. Lam, Inhaled RNA therapy: From promise to reality. *Trends Pharmacol. Sci.* **41**, 715–729 (2020).

8. I. Sahu, A. Haque, B. Weidensee, P. Weinmann, M. S. D. Kormann, Recent developments in mRNA-based protein supplementation therapy to target lung diseases. *Mol. Ther.* **27**, 803–823 (2019).
9. J. Tang, L. Cai, C. Xu, S. Sun, Y. Liu, J. Rosenecker, S. Guan, Nanotechnologies in delivery of DNA and mRNA vaccines to the nasal and pulmonary mucosa. *Nanomaterials* **12**, 226 (2022).
10. N. Pardi, S. Tuyishime, H. Muramatsu, K. Kariko, B. L. Mui, Y. K. Tam, T. D. Madden, M. J. Hope, D. Weissman, Expression kinetics of nucleoside-modified mRNA delivered in lipid nanoparticles to mice by various routes. *J. Control. Release* **217**, 345–351 (2015).
11. S. M. Rowe, J. B. Zuckerman, D. Dorgan, J. Lascano, K. McCoy, M. Jain, M. S. Schechter, S. Lommatzsch, V. Indihar, N. Lechtzin, K. McBennett, C. Callison, C. Brown, T. G. Liou, K. D. MacDonald, S. Z. Nasr, S. Bodie, M. Vaughn, E. B. Meltzer, A. J. Barbier, Inhaled mRNA therapy for treatment of cystic fibrosis: Interim results of a randomized, double-blind, placebo-controlled phase 1/2 clinical study. *J. Cyst. Fibros.*, 10.1016/j.jcf.2023.04.008 (2023).
12. M. Mutsch, W. Zhou, P. Rhodes, M. Bopp, R. T. Chen, T. Linder, C. Spyr, R. Steffen, Use of the inactivated intranasal influenza vaccine and the risk of Bell's palsy in Switzerland. *N. Engl. J. Med.* **350**, 896–903 (2004).
13. S. Ndeupen, Z. Qin, S. Jacobsen, A. Bouteau, H. Estanbouli, B. Z. Igyártó, The mRNA-LNP platform's lipid nanoparticle component used in preclinical vaccine studies is highly inflammatory. *iScience* **24**, 103479 (2021).
14. J. Zhou, J. Liu, C. J. Cheng, T. R. Patel, C. E. Weller, J. M. Piepmeier, Z. Jiang, W. M. Saltzman, Biodegradable poly(amine-*co*-ester) terpolymers for targeted gene delivery. *Nat. Mater.* **11**, 82–90 (2011).
15. A. C. Kauffman, A. S. Piotrowski-Daspit, K. H. Nakazawa, Y. Jiang, A. Datye, W. M. Saltzman, Tunability of biodegradable poly(amine-*co*-ester) polymers for customized nucleic acid delivery and other biomedical applications. *Biomacromolecules* **19**, 3861–3873 (2018).
16. Y. Jiang, Q. Lu, Y. Wang, E. Xu, A. Ho, P. Singh, Y. Wang, Z. Jiang, F. Yang, G. T. Tietjen, P. Cresswell, W. M. Saltzman, Quantitating endosomal escape of a library of polymers for mRNA delivery. *Nano Lett.* **20**, 1117–1123 (2020).
17. M. K. Grun, A. Suberi, K. Shin, T. Lee, V. Gomerdinger, Z. M. Moscato, A. S. Piotrowski-Daspit, W. M. Saltzman, PEGylation of poly(amine-co-ester) polyplexes for tunable gene delivery. *Biomaterials* **272**, 120780 (2021).
18. X. Zhang, B. Liu, Z. Yang, C. Zhang, H. Li, X. Luo, H. Luo, D. Gao, Q. Jiang, J. Liu, Z. Jiang, Micelles of enzymatically synthesized PEG-poly(amine-*co*-ester) block copolymers as pH-responsive nanocarriers for docetaxel delivery. *Colloids Surf. B Biointerfaces* **115**, 349–358 (2014).
19. M. Ogris, S. Brunner, S. Schüller, R. Kircheis, E. Wagner, PEGylated DNA/transferrin-PEI complexes: Reduced interaction with blood components, extended circulation in blood and potential for systemic gene delivery. *Gene Ther.* **6**, 595–605 (1999).
20. D. Oupicky, M. Ogris, K. A. Howard, P. R. Dash, K. Ulbrich, L. W. Seymour, Importance of lateral and steric stabilization of polyelectrolyte gene delivery vectors for extended systemic circulation. *Mol. Ther.* **5**, 463–472 (2002).
21. S. J. Sung, S. H. Min, K. Y. Cho, S. Lee, Y. J. Min, Y. I. Yeom, J. K. Park, Effect of polyethylene glycol on gene delivery of polyethylenimine. *Biol. Pharm. Bull.* **26**, 492–500 (2003).
22. Z. T. Cao, L. Q. Gan, W. Jiang, J. L. Wang, H. B. Zhang, Y. Zhang, Y. Wang, X. Yang, M. Xiong, J. Wang, Protein binding affinity of polymeric nanoparticles as a direct indicator of their pharmacokinetics. *ACS Nano* **14**, 3563–3575 (2020).
23. S. Li, Y. Hu, A. Li, J. Lin, K. Hsieh, Z. Schneiderman, P. Zhang, Y. Zhu, C. Qiu, E. Kokkoli, T.-H. Wang, H.-Q. Mao, Payload distribution and capacity of mRNA lipid nanoparticles. *Nat. Commun.* **13**, 5561 (2022).
24. G. Osman, J. Rodriguez, S. Y. Chan, J. Chisholm, G. Duncan, N. Kim, A. L. Tatler, K. M. Shakesheff, J. Hanes, J. S. Suk, J. E. Dixon, PEGylated enhanced cell penetrating peptide nanoparticles for lung gene therapy. *J. Control. Release* **285**, 35–45 (2018).
25. C. E. Nelson, J. R. Kintzing, A. Hanna, J. M. Shannon, M. K. Gupta, C. L. Duvall, Balancing cationic and hydrophobic content of PEGylated siRNA polyplexes enhances endosome escape, stability, blood circulation time, and bioactivity in vivo. *ACS Nano* **7**, 8870–8880 (2013).
26. J. C. Kaczmarek, K. J. Kauffman, O. S. Fenton, K. Sadtler, A. K. Patel, M. W. Heartlein, F. DeRosa, D. G. Anderson, Optimization of a degradable polymer-lipid nanoparticle for potent systemic delivery of mRNA to the lung endothelium and immune cells. *Nano Lett.* **18**, 6449–6454 (2018).
27. Y. Cu, W. M. Saltzman, Controlled surface modification with poly(ethylene)glycol enhances diffusion of PLGA nanoparticles in human cervical mucus. *Mol. Pharm.* **6**, 173–181 (2009).
28. A. V. Li, J. J. Moon, W. Abraham, H. Suh, J. Elkhader, M. A. Seidman, M. Yen, E. J. Im, M. H. Foley, D. H. Barouch, D. J. Irvine, Generation of effector memory T cell-based mucosal and systemic immunity with pulmonary nanoparticle vaccination. *Sci. Transl. Med.* **5**, 204ra130 (2013).
29. K. Rakhra, W. Abraham, C. Wang, K. D. Moynihan, N. Li, N. Donahue, A. D. Baldeon, D. J. Irvine, Exploiting albumin as a mucosal vaccine chaperone for robust generation of lung-resident memory T cells. *Sci. Immunol.* **6**, eabd8003 (2021).
30. G. Ortiz-Muñoz, M. R. Looney, Non-invasive intratracheal instillation in mice. *Bio Protoc.* **5**, e1504 (2015).
31. A. K. Patel, J. C. Kaczmarek, S. Bose, K. J. Kauffman, F. Mir, M. W. Heartlein, F. DeRosa, R. Langer, D. G. Anderson, Inhaled nanoformulated mRNA polyplexes for protein production in lung epithelium. *Adv. Mater.* **31**, e1805116 (2019).
32. E. S. Winkler, A. L. Bailey, N. M. Kafai, S. Nair, B. T. McCune, J. Yu, J. M. Fox, R. E. Chen, J. T. Earnest, S. P. Keeler, J. H. Ritter, L.-I. Kang, S. Dort, A. Robichaud, R. Head, M. J. Holtzman, M. S. Diamond, SARS-CoV-2 infection of human ACE2-transgenic mice causes severe lung inflammation and impaired function. *Nat. Immunol.* **21**, 1327–1335 (2020).
33. T. Mao, B. Israelow, M. A. Peña-Hernández, A. Suberi, L. Zhou, S. Luyten, M. Reschke, H. Dong, R. J. Homer, W. M. Saltzman, A. Iwasaki, Unadjuvanted intranasal spike vaccine elicits protective mucosal immunity against sarbecoviruses. *Science* **378**, eabo2523 (2022).
34. S. Afkhami, M. R. D'Agostino, A. Zhang, H. D. Stacey, A. Marzok, A. Kang, R. Singh, J. Bavananthasivam, G. Ye, X. Luo, F. Wang, J. C. Ang, A. Zganiacz, U. Sankar, N. Kazhdan, J. F. E. Koenig, A. Phelps, S. F. Gameiro, S. Tang, M. Jordana, Y. Wan, K. L. Mossman, M. Jeyanathan, A. Gillgrass, M. F. C. Medina, F. Smaill, B. D. Lichty, M. S. Miller, Z. Xing, Respiratory mucosal delivery of next-generation COVID-19 vaccine provides robust protection against both ancestral and variant strains of SARS-CoV-2. *Cell* **185**, 896–915.e19 (2022).
35. B. Israelow, T. Mao, J. Klein, E. Song, B. Menasche, S. B. Omer, A. Iwasaki, Adaptive immune determinants of viral clearance and protection in mouse models of SARS-CoV-2. *Sci. Immunol.* **6**, eabl4509 (2021).
36. F. C. Knight, J. T. Wilson, Engineering vaccines for tissue-resident memory T cells. *Adv. Ther.* **4**, 2000230 (2021).
37. S. R. Allie, J. E. Bradley, U. Mudunuru, M. D. Schultz, B. A. Graf, F. E. Lund, T. D. Randall, The establishment of resident memory B cells in the lung requires local antigen encounter. *Nat. Immunol.* **20**, 97–108 (2019).
38. J. K. Krishnaswamy, S. Alsén, U. Yrlid, S. C. Eisenbarth, A. Williams, Determination of T follicular helper cell fate by dendritic cells. *Front. Immunol.* **9**, 2169 (2018).
39. K. Lederer, D. Castaño, D. Gómez Atria, T. H. Oguin III, S. Wang, T. B. Manzoni, H. Muramatsu, M. J. Hogan, F. Amanat, P. Cherubin, K. A. Lundgreen, Y. K. Tam, S. H. Y. Fan, L. C. Eisenlohr, I. Maillard, D. Weissman, P. Bates, F. Krammer, G. D. Sempowski, N. Pardi, M. Locci, SARS-CoV-2 mRNA vaccines foster potent antigen-specific germinal center responses associated with neutralizing antibody generation. *Immunity* **53**, 1281–1295.e5 (2020).
40. J. S. Turner, J. A. O'Halloran, E. Kalaidina, W. Kim, A. J. Schmitz, J. Q. Zhou, T. Lei, M. Thapa, R. E. Chen, J. B. Case, F. Amanat, A. M. Rauseo, A. Haile, X. Xie, M. K. Klebert, T. Suessen, W. D. Middleton, P. Y. Shi, F. Krammer, S. A. Teefey, M. S. Diamond, R. M. Presti, A. H. Ellebedy, SARS-CoV-2 mRNA vaccines induce persistent human germinal centre responses. *Nature* **596**, 109–113 (2021).
41. M. P. Lokugamage, D. Vanover, J. Beyersdorf, M. Z. C. Hatit, L. Rotolo, E. S. Echeverri, H. E. Peck, H. Ni, J. K. Yoon, Y. Kim, P. J. Santangelo, J. E. Dahlman, Optimization of lipid nanoparticles for the delivery of nebulized therapeutic mRNA to the lungs. *Nat. Biomed. Eng.* **5**, 1059–1068 (2021).
42. K. J. Kauffman, J. R. Dorkin, J. H. Yang, M. W. Heartlein, F. DeRosa, F. F. Mir, O. S. Fenton, D. G. Anderson, Optimization of lipid nanoparticle formulations for mrna delivery in vivo with fractional factorial and definitive screening designs. *Nano Lett.* **15**, 7300–7306 (2015).
43. H. Zhang, J. Leal, M. R. Soto, H. D. C. Smyth, D. Ghosh, Aerosolizable lipid nanoparticles for pulmonary delivery of mRNA through design of experiments. *Pharmaceutics* **12**, 1042 (2020).
44. B. Li, R. S. Manan, S.-Q. Liang, A. Gordon, A. Jiang, A. Varley, G. Gao, R. Langer, W. Xue, D. Anderson, Combinatorial design of nanoparticles for pulmonary mRNA delivery and genome editing. *Nat. Biotechnol.* 10.1038/s41587-023-01679-x, (2023).
45. J. T. Huckaby, S. K. Lai, PEGylation for enhancing nanoparticle diffusion in mucus. *Adv. Drug Deliv. Rev.* **124**, 125–139 (2018).
46. A. Jarzębińska, T. Pasewald, J. Lambrecht, O. Mykhaylyk, L. Kümmerling, P. Beck, G. Hasenpusch, C. Rudolph, C. Plank, C. Dohmen, A single methylene group in oligoalkylamine-based cationic polymers and lipids promotes enhanced mRNA delivery. *Angew. Chem. Int. Ed. Engl.* **55**, 9591–9595 (2016).
47. P. S. Kowalski, U. Capasso Palmiero, Y. Huang, A. Rudra, R. Langer, D. G. Anderson, Ionizable amino-polyesters synthesized via ring opening polymerization of tertiary amino-alcohols for tissue selective mRNA delivery. *Adv. Mater.* **30**, e1801151 (2018).
48. L. Rotolo, D. Vanover, N. C. Bruno, H. E. Peck, C. Zurla, J. Murray, R. K. Noel, L. O'Farrell, M. Araínga, N. Orr-Burks, J. Y. Joo, L. C. S. Chaves, Y. Jung, J. Beyersdorf, S. Gumber, R. Guerrero-Ferreira, S. Cornejo, M. Thoresen, A. K. Olivier, K. M. Kuo, J. C. Gumbart, A. R. Woolums, F. Villinger, E. R. Lafontaine, R. J. Hogan, M. G. Finn, P. J. Santangelo, Species-

agnostic polymeric formulations for inhalable messenger RNA delivery to the lung. *Nat. Mater.* **22**, 369–379 (2022).

49. Q. Cheng, T. Wei, L. Farbiak, L. T. Johnson, S. A. Dilliard, D. J. Siegwart, Selective organ targeting (SORT) nanoparticles for tissue-specific mRNA delivery and CRISPR-Cas gene editing. *Nat. Nanotechnol.* **15**, 313–320 (2020).
50. M. Qiu, Y. Tang, J. Chen, R. Muriph, Z. Ye, C. Huang, J. Evans, E. P. Henske, Q. Xu, Lung-selective mRNA delivery of synthetic lipid nanoparticles for the treatment of pulmonary lymphangioleiomyomatosis. *Proc. Natl. Acad. Sci. U.S.A.* **119**, e2116271119 (2022).
51. A. Da Silva Sanchez, K. Paunovska, A. Cristian, J. E. Dahlman, Treating cystic fibrosis with mRNA and CRISPR. *Hum. Gene Ther.* **31**, 940–955 (2020).
52. S. Guan, A. Munder, S. Hedtfeld, P. Braubach, S. Glage, L. Zhang, S. Lienenklaus, A. Schultze, G. Hasenpusch, W. Garrels, F. Stanke, C. Miskey, S. M. Johler, Y. Kumar, B. Tümmler, C. Rudolph, Z. Ivics, J. Rosenecker, Self-assembled peptide-poloxamine nanoparticles enable in vitro and in vivo genome restoration for cystic fibrosis. *Nat. Nanotechnol.* **14**, 287–297 (2019).
53. F. Zeyer, B. Mothes, C. Will, M. Carevic, J. Rottenberger, B. Nürnberg, D. Hartl, R. Handgretinger, S. Beer-Hammer, M. S. Kormann, mRNA-mediated gene supplementation of toll-like receptors as treatment strategy for asthma in vivo. *PLOS ONE* **11**, e0154001 (2016).
54. M. S. Kormann, G. Hasenpusch, M. K. Aneja, G. Nica, A. W. Flemmer, S. Herber-Jonat, M. Huppmann, L. E. Mays, M. Illenyi, A. Schams, M. Griese, I. Bittmann, R. Handgretinger, D. Hartl, J. Rosenecker, C. Rudolph, Expression of therapeutic proteins after delivery of chemically modified mRNA in mice. *Nat. Biotechnol.* **29**, 154–157 (2011).
55. S. Guan, M. Darmstädter, C. Xu, J. Rosenecker, In vitro investigations on optimizing and nebulization of IVT-mRNA formulations for potential pulmonary-based alpha-1-antitrypsin deficiency treatment. *Pharmaceutics* **13**, 1281 (2021).
56. A. E. Potash, T. J. Wallen, P. H. Karp, S. Ernst, T. O. Moninger, N. D. Gansemer, D. A. Stoltz, J. Zabner, E. H. Chang, Adenoviral gene transfer corrects the ion transport defect in the sinus epithelia of a porcine CF model. *Mol. Ther.* **21**, 947–953 (2013).
57. A. Haque, A. Dewerth, J. S. Antony, J. Riethmüller, G. R. Schweizer, P. Weinmann, N. Latifi, H. Yasar, N. Pedemonte, E. Sondo, B. Weidensee, A. Ralhan, J. Laval, P. Schlegel, C. Seitz, B. Loretz, C. M. Lehr, R. Handgretinger, M. S. D. Kormann, Chemically modified hCFTR mRNAs recuperate lung function in a mouse model of cystic fibrosis. *Sci. Rep.* **8**, 16776 (2018).
58. E. Robinson, K. D. MacDonald, K. Slaughter, M. McKinney, S. Patel, C. Sun, G. Sahay, Lipid nanoparticle-delivered chemically modified mRNA restores chloride secretion in cystic fibrosis. *Mol. Ther.* **26**, 2034–2046 (2018).
59. C. Lucas, C. B. F. Vogels, I. Yildirim, J. E. Rothman, P. Lu, V. Monteiro, J. R. Gehlhausen, M. Campbell, J. Silva, A. Tabachnikova, M. A. Peña-Hernandez, M. C. Muenker, M. I. Breban, J. R. Fauver, S. Mohanty, J. Huang; Yale SARS-CoV-2 Genomic Surveillance Initiative, A. C. Shaw, A. I. Ko, S. B. Omer, N. D. Grubaugh, A. Iwasaki, Impact of circulating SARS-CoV-2 variants on mRNA vaccine-induced immunity. *Nature* **600**, 523–529 (2021).
60. J. Lopez Bernal, N. Andrews, C. Gower, E. Gallagher, R. Simmons, S. Thelwall, J. Stowe, E. Tessier, N. Groves, G. Dabrera, R. Myers, C. N. J. Campbell, G. Amirthalingam, M. Edmunds, M. Zambon, K. E. Brown, S. Hopkins, M. Chand, M. Ramsay, Effectiveness of Covid-19 vaccines against the B.1.617.2 (Delta) variant. *N. Engl. J. Med.* **385**, 585–594 (2021).
61. K. J. Bruxvoort, L. S. Sy, L. Qian, B. K. Ackerson, Y. Luo, G. S. Lee, Y. Tian, A. Florea, M. Aragones, J. E. Tubert, H. S. Takhar, J. H. Ku, Y. D. Paila, C. A. Talarico, H. F. Tseng, Effectiveness of mRNA-1273 against delta, mu, and other emerging variants of SARS-CoV-2: Test negative case-control study. *BMJ* **375**, e068848 (2021).
62. S. Collie, J. Champion, H. Moultrie, L. G. Bekker, G. Gray, Effectiveness of BNT162b2 vaccine against omicron variant in South Africa. *N. Engl. J. Med.* **386**, 494–496 (2022).
63. J. M. Ferdinands, S. Rao, B. E. Dixon, P. K. Mitchell, M. B. De Silva, S. A. Irving, N. Lewis, K. Natarajan, E. Stenehjem, S. J. Grannis, J. Han, C. M. Evoy, T. C. Ong, A. L. Naleway, S. E. Reese, P. J. Embi, K. Dascomb, N. P. Klein, E. P. Griggs, D. Konatham, A. B. Kharbanda, D.-H. Yang, W. F. Fadel, N. Grisel, K. Goddard, P. Patel, I.-C. Liao, R. Birch, N. R. Valvi, S. Reynolds, J. Arndorfer, O. Zerbo, M. Dickerson, K. Murthy, J. Williams, C. H. Bozio, L. Blanton, J. R. Verani, S. J. Schrag, A. F. Dalton, M. H. Wondimu, R. Link-Gelles, E. Azziz-Baumgartner, M. A. Barron, M. Gaglani, M. G. Thompson, B. Fireman, Waning 2-dose and 3-dose effectiveness of mRNA vaccines against COVID-19–associated emergency department and urgent care encounters and hospitalizations among adults during periods of delta and omicron variant predominance—VISION Network, 10 States, August 2021–January 2022. *MMWR Morb. Mortal. Wkly. Rep.* **71**, 255–263 (2022).
64. R. Rubin, COVID-19 boosters this fall to include omicron antigen, but questions remain about its value. *JAMA* **328**, 412–414 (2022).
65. K. S. Corbett, D. K. Edwards, S. R. Leist, O. M. Abiona, S. Boyoglu-Barnum, R. A. Gillespie, S. Himansu, A. Schäfer, C. T. Ziwawo, A. T. DiPiazza, K. H. Dinnon, S. M. Elbashir, C. A. Shaw, A. Woods, E. J. Fritch, D. R. Martinez, K. W. Bock, M. Minai, B. M. Nagata, G. B. Hutchinson, K. Wu, C. Henry, K. Bahl, D. Garcia-Dominguez, L. Ma, I. Renzi, W.-P. Kong, S. D. Schmidt, L. Wang, Y. Zhang, E. Phung, L. A. Chang, R. J. Loomis, N. E. Altaras, E. Narayanan, M. Metkar, V. Presnyak, C. Liu, M. K. Louder, W. Shi, K. Leung, E. S. Yang, A. West, K. L. Gully, L. J. Stevens, N. Wang, D. Wrapp, N. A. Doria-Rose, G. Stewart-Jones, H. Bennett, G. S. Alvarado, M. C. Nason, T. J. Ruckwardt, J. S. McLellan, M. R. Denison, J. D. Chappell, I. N. Moore, K. M. Morabito, J. R. Mascola, R. S. Baric, A. Carfi, B. S. Graham, SARS-CoV-2 mRNA vaccine design enabled by prototype pathogen preparedness. *Nature* **586**, 567–571 (2020).
66. A. B. Vogel, I. Kanevsky, Y. Che, K. A. Swanson, A. Muik, M. Vormehr, L. M. Kranz, K. C. Walzer, S. Hein, A. Güler, J. Loschko, M. S. Maddur, A. Ota-Setlik, K. Tompkins, J. Cole, B. G. Lui, T. Ziegenhals, A. Plaschke, D. Eisel, S. C. Dany, S. Fesser, S. Erbar, F. Bates, D. Schneider, B. Jesionek, B. Sänger, A.-K. Wallisch, Y. Feuchter, H. Junginger, S. A. Krumm, A. P. Heinen, P. Adams-Quack, J. Schlereth, S. Schille, C. Kröner, R. de la Caridad Güimil Garcia, T. Hiller, L. Fischer, R. S. Sellers, S. Choudhary, O. Gonzalez, F. Vascotto, M. R. Gutman, J. A. Fontenot, S. Hall-Ursone, K. Brasky, M. C. Griffor, S. Han, A. A. H. Su, J. A. Lees, N. L. Nedoma, E. H. Mashalidis, P. V. Sahasrabudhe, C. Y. Tan, D. Pavliakova, G. Singh, C. Fontes-Garfias, M. Pride, I. L. Scully, T. Ciolino, J. Obregon, M. Gazi, R. Carrion, K. J. Alfson, W. V. Kalina, D. Kaushal, P.-Y. Shi, T. Klamp, C. Rosenbaum, A. N. Kuhn, Ö. Türeci, P. R. Dormitzer, K. U. Jansen, U. Sahin, BNT162b vaccines protect rhesus macaques from SARS-CoV-2. *Nature* **592**, 283–289 (2021).
67. R. Heida, W. L. Hinrichs, H. W. Frijlink, Inhaled vaccine delivery in the combat against respiratory viruses: A 2021 overview of recent developments and implications for COVID-19. *Expert Rev. Vaccines* **21**, 957–974 (2022).
68. E. J. Topol, A. Iwasaki, Operation nasal vaccine-lightning speed to counter COVID-19. *Sci. Immunol.* **7**, eadd9947 (2022).
69. N. van Doremalen, J. N. Purushotham, J. E. Schulz, M. G. Holbrook, T. Bushmaker, A. Carmody, J. R. Port, C. K. Yinda, A. Okumura, G. Saturday, F. Amanat, F. Krammer, P. W. Hanley, B. J. Smith, J. Lovaglio, S. L. Anzick, K. Barbian, C. Martens, S. C. Gilbert, T. Lambe, V. J. Munster, Intranasal ChAdOx1 nCoV-19/AZD1222 vaccination reduces viral shedding after SARS-CoV-2 D614G challenge in preclinical models. *Sci. Transl. Med.* **13**, eabh0755 (2021).
70. D. An, K. Li, D. K. Rowe, M. C. H. Diaz, E. F. Griffin, A. C. Beavis, S. K. Johnson, I. Padykula, C. A. Jones, K. Briggs, G. Li, Y. Lin, J. Huang, J. Mousa, M. Brindley, K. Sakamoto, D. K. Meyerholz, P. B. McCray Jr., S. M. Tompkins, B. He, Protection of K18-hACE2 mice and ferrets against SARS-CoV-2 challenge by a single-dose mucosal immunization with a parainfluenza virus 5-based COVID-19 vaccine. *Sci. Adv.* **7**, eabi5246 (2021).
71. A. O. Hassan, N. M. Kafai, I. P. Dmitriev, J. M. Fox, B. K. Smith, I. B. Harvey, R. E. Chen, E. S. Winkler, A. W. Wessel, J. B. Case, E. Kashentseva, B. T. McCune, A. L. Bailey, H. Zhao, L. A. VanBlargan, Y. N. Dai, M. Ma, L. J. Adams, S. Shrihari, J. E. Danis, L. E. Gralinski, Y. J. Hou, A. Schäfer, A. S. Kim, S. P. Keeler, D. Weiskopf, R. S. Baric, M. J. Holtzman, D. H. Fremont, D. T. Curiel, M. S. Diamond, A single-dose intranasal ChAd vaccine protects upper and lower respiratory tracts against SARS-CoV-2. *Cell* **183**, 169–184.e13 (2020).
72. J. E. Oh, E. Song, M. Moriyama, P. Wong, S. Zhang, R. Jiang, S. Strohmeier, S. H. Kleinstein, F. Krammer, A. Iwasaki, Intranasal priming induces local lung-resident B cell populations that secrete protective mucosal antiviral IgA. *Sci. Immunol.* **6**, eabj5129 (2021).
73. R. Yuan, J. Yu, Z. Jiao, J. Li, F. Wu, R. Yan, X. Huang, C. Chen, The roles of tissue-resident memory T cells in lung diseases. *Front. Immunol.* **12**, 710375 (2021).
74. J. Tang, C. Zeng, T. M. Cox, C. Li, Y. M. Son, I. S. Cheon, Y. Wu, S. Behl, J. J. Taylor, R. Chakaraborty, A. J. Johnson, D. N. Shiavo, J. P. Utz, J. S. Reisenauer, D. E. Midthun, J. J. Mullon, E. S. Edell, M. G. Alameh, L. Borish, W. G. Teague, M. H. Kaplan, D. Weissman, R. Kern, H. Hu, R. Vassallo, S.-L. Liu, J. Sun, Respiratory mucosal immunity against SARS-CoV-2 after mRNA vaccination. *Sci. Immunol.* **7**, eadd4853 (2022).
75. E. L. Blanchard, D. Vanover, S. S. Bawage, P. M. Tiwari, L. Rotolo, J. Beyersdorf, H. E. Peck, N. C. Bruno, R. Hincapie, F. Michel, J. Murray, H. Sadhwani, B. Vanderheyden, M. G. Finn, M. A. Brinton, E. R. Lafontaine, R. J. Hogan, C. Zurla, P. J. Santangelo, Treatment of influenza and SARS-CoV-2 infections via mRNA-encoded Cas13a in rodents. *Nat. Biotechnol.* **39**, 717–726 (2021).
76. J. Kim, A. Jozic, A. Mukherjee, D. Nelson, K. Chiem, M. S. R. Khan, J. B. Torrelles, L. Martinez-Sobrido, G. Sahay, Rapid generation of circulating and mucosal decoy human ACE2 using mRNA nanotherapeutics for the potential treatment of SARS-CoV-2. *Adv Sci (Weinh)* **9**, 2202556 (2022).
77. J. Q. Li, Z. R. Zhang, H. Q. Zhang, Y. N. Zhang, X. Y. Zeng, Q. Y. Zhang, C. L. Deng, X. D. Li, B. Zhang, H. Q. Ye, Intranasal delivery of replicating mRNA encoding neutralizing antibody against SARS-CoV-2 infection in mice. *Signal Transduct. Target. Ther.* **6**, 369 (2021).
78. D. Vanover, C. Zurla, H. E. Peck, N. Orr-Burks, J. Y. Joo, J. Murray, N. Holladay, R. A. Hobbs, Y. Jung, L. C. S. Chaves, L. Rotolo, A. W. Lifland, A. K. Olivier, D. Li, K. O. Saunders, G. D. Sempowski, J. E. Crowe Jr., B. F. Haynes, E. R. Lafontaine, R. J. Hogan, P. J. Santangelo, Nebulized mRNA-encoded antibodies protect hamsters from SARS-CoV-2 infection. *Adv. Sci.* **9**, e2202771 (2022).
79. G. Repetto, A. del Peso, J. L. Zurita, Neutral red uptake assay for the estimation of cell viability/cytotoxicity. *Nat. Protoc.* **3**, 1125–1131 (2008).

80. B. Israelow, E. Song, T. Mao, P. Lu, A. Meir, F. Liu, M. M. Alfajaro, J. Wei, H. Dong, R. J. Homer, A. Ring, C. B. Wilen, A. Iwasaki, Mouse model of SARS-CoV-2 reveals inflammatory role of type I interferon signaling. *J. Exp. Med.* **217**, e20201241 (2020).
81. T. Mao, B. Israelow, C. Lucas, C. B. F. Vogels, M. L. Gomez-Calvo, O. Fedorova, M. I. Breban, B. L. Menasche, H. Dong, M. Linehan, C. B. Wilen, M. L. Landry, N. D. Grubaugh, A. M. Pyle, A. Iwasaki, A stem-loop RNA RIG-I agonist protects against acute and chronic SARS-CoV-2 infection in mice. *J. Exp. Med.* **219**, e20211818 (2022).
82. L. Shi, J. Zhang, M. Zhao, S. Tang, X. Cheng, W. Zhang, W. Li, X. Liu, H. Peng, Q. Wang, Effects of polyethylene glycol on the surface of nanoparticles for targeted drug delivery. *Nanoscale* **13**, 10748–10764 (2021).
83. E. Padín-González, P. Lancaster, M. Bottini, P. Gasco, L. Tran, B. Fadeel, T. Wilkins, M. P. Monopoli, Understanding the role and impact of poly(ethylene glycol) (PEG) on nanoparticle formulation: Implications for COVID-19 vaccines. *Front. Bioeng. Biotechnol.* **10**, 882363 (2022).
84. M. Maurel, T. Montheil, J. Martin, L. Chaar, V. Guzman-Gonzalez, M. Couvet, T. Jacquet, T. Jia, B. Eymin, K. Parra, P. Dumy, J. Martinez, F. Ruggiero, E. Vaganay, A. Mehdi, J. L. Coll, G. Subra, Design of PEGylated three ligands silica nanoparticles for multi-receptor targeting. *Nanomaterials* **11**, 177 (2021).
85. Q. Xu, L. M. Ensign, N. J. Boylan, A. Schön, X. Gong, J. C. Yang, N. W. Lamb, S. Cai, T. Yu, E. Freire, J. Hanes, Impact of surface polyethylene glycol (PEG) density on biodegradable nanoparticle transport in mucus ex vivo and distribution in vivo. *ACS Nano* **9**, 9217–9227 (2015).

Acknowledgments: Graphical illustrations were created with Biorender.com. We thank the NIH tetramer Core Facility for providing phycoerythrin-labeled SARS-CoV-2 S 539-546 tetramer [H-2 K(b)] and allophycocyanin-labeled S 62-76 MHC class II tetramer [I-A(b)]. The following reagent was obtained through BEI Resources, NIAID, NIH: *Cercopithecus aethiops* kidney epithelial cells expressing transmembrane protease, serine 2, and human angiotensin-converting enzyme 2 (Vero E6-TMPRSS2-T2A-ACE2), NR-54970. The following reagent was deposited by the Centers for Disease Control and Prevention and obtained through BEI Resources, NIAID, NIH: SARS-related coronavirus 2, isolate hCoV-19/USA-WA1/2020, NR-52281. **Funding:** This work was supported by NIH grants UG3 HL147352 (W.M.S.) and R01 AI157488 (A.I.), the Fast Grant from Emergent Ventures at the Mercatus Center (A.I.), and HHMI funding dedicated to collaborative research projects on SARS-CoV-2 and the disease that it causes, COVID-19 (A.I.). A.S. is supported by the NIGMS T32GM136651. A.I. is an Investigator of the Howard Hughes Medical Institute. B.I. is supported by NIAID T32AI007517 and K08AI163493. T.M. is supported by NIAID T32AI007019. A.S.P.-D. is supported by a K99/R00 Pathway to Independence award from the NIH (K99 HL151806) and a Postdoc-to-Faculty Transition Award from the Cystic Fibrosis Foundation (CFF; PIOTRO21F5). **Author contributions:** A.S., A.I., and W.M.S. conceptualized the study. A.S., M.K.G., H.-W.S., T.M., B.I., M.R., J.G., and T.L. developed the methodology. A.S., M.K.G., H.-W.S., T.M., B.I., M.R., J.G., L.A., T.L., K.S., A.S.P.-D., and R.J.H. performed experiments. A.S., M.K.G., T.M., and B.I. analyzed and interpreted results. A.I., H.-W.S., and W.M.S. supervised the project. A.S. wrote the original draft that was reviewed and revised by all authors. **Competing interests:** A.S.P.-D., A.I., and W.M.S. are cofounders of Xanadu Bio, and B.I. and T.M. serve as consultants for Xanadu Bio. A.I., B.I., T.M., W.M.S., A.S., M.R., A.S.P.-D., and H.-W.S. are listed as inventors on patent applications relating to intranasal PACE SARS-CoV-2 vaccines filed by Yale University (Nanoparticle immunogenic compositions and vaccination methods, PCT/US2022/081199). W.M.S. is listed as inventor on patent applications relating to end group–modified PACE NPs filed by Yale University [Poly(amine-*co*-ester) polymers and polyplexes with modified end groups and methods of use thereof, 16/862,491]. A.S., M.K.G., and W.M.S. are listed as inventors on patent applications relating to PACE-mRNA delivery to the lung filed by Yale University [Poly(amine-*co*-ester) polymers with modified end groups and enhanced pulmonary delivery, 18/002,241]. **Data and materials availability:** All data associated with this study are present in the paper or the Supplementary Materials. Requests for data should be addressed to H.-W.S. or W.M.S. Reagents used to conduct these experiments are either publicly available as detailed in Materials and Methods or available with appropriate material transfer agreements. PACE polymers synthesized for this project are available from W.M.S. under a material transfer agreement with Yale University.

Submitted 22 March 2022
Resubmitted 13 March 2023
Accepted 26 June 2023
Published 16 August 2023
10.1126/scitranslmed.abq0603

Science Translational Medicine

Polymer nanoparticles deliver mRNA to the lung for mucosal vaccination

Alexandra Suberi, Molly K. Grun, Tianyang Mao, Benjamin Israelow, Melanie Reschke, Julian Grundler, Laiba Akhtar, Teresa Lee, Kwangsoo Shin, Alexandra S. Piotrowski-Daspit, Robert J. Homer, Akiko Iwasaki, Hee-Won Suh, and W. Mark Saltzman

Sci. Transl. Med. **15** (709), eabq0603. DOI: 10.1126/scitranslmed.abq0603